Nucleic Acids Research, 2024, **52**, 3069–3087
https://doi.org/10.1093/nar/gkae031
Advance access publication date: 7 February 2024
Genome integrity, repair and replication

DNA hypomethylation activates Cdk4/6 and Atr to induce DNA replication and cell cycle arrest to constrain liver outgrowth in zebrafish

Bhavani P. Madakashira, Elena Magnani, Shashi Ranjan and Kirsten C. Sadler*

Program in Biology NYU Abu Dhabi, Abu Dhabi, UAE

*To whom correspondence should be addressed. Tel: +971 2 628 4569; Email: kirsten.edepli@nyu.edu

Abstract

Coordinating epigenomic inheritance and cell cycle progression is essential for organogenesis. UHRF1 connects these functions during development by facilitating maintenance of DNA methylation and cell cycle progression. Here, we provide evidence resolving the paradoxical phenotype of *uhrf1* mutant zebrafish embryos which have activation of pro-proliferative genes and increased number of hepatocytes in S-phase, but the liver fails to grow. We uncover decreased Cdkn2a/b and persistent Cdk4/6 activation as the mechanism driving *uhrf1* mutant hepatocytes into S-phase. This induces replication stress, DNA damage and Atr activation. Palbociclib treatment of *uhrf1* mutants prevented aberrant S-phase entry, reduced DNA damage, and rescued most cellular and developmental phenotypes, but it did not rescue DNA hypomethylation, transposon expression or the interferon response. Inhibiting Atr reduced DNA replication and increased liver size in *uhrf1* mutants, suggesting that Atr activation leads to dormant origin firing and prevents hepatocyte proliferation. Cdkn2a/b was downregulated pro-proliferative genes were also induced in a Cdk4/6 dependent fashion in the liver of *dnmt1* mutants, suggesting DNA hypomethylation as a mechanism of Cdk4/6 activation during development. This shows that the developmental defects caused by DNA hypomethylation are attributed to persistent Cdk4/6 activation, DNA replication stress, dormant origin firing and cell cycle inhibition.

Graphical abstract

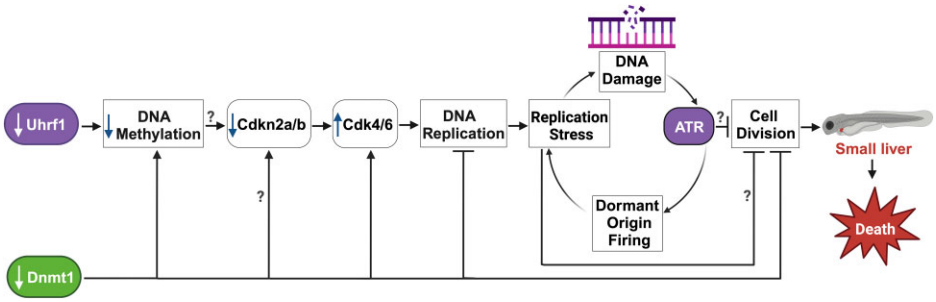

Introduction

Cell proliferation during organogenesis requires precise coordination of the machinery that replicates the genome with those that pattern the epigenome. During S-phase, both CpG density and the chromatin landscape influence when, where and the efficiency with which the origins of replication fire (1,2). Widespread changes to the epigenome change this landscape, and thus the epigenetic repatterning that occur during development, aging or in cancer can influence the pattern, timing and successful progression of DNA replication (3,4). The mechanism by which cells in the developing embryo couple epigenetic patterning with efficient DNA replication is not well understood.

DNA methylation is the best studied epigenetic mark. There is little variation in the DNA methylation pattern across healthy somatic cells as in nearly all cell types, it is enriched on CpG-dense transposons and absent from CpG islands in promoters. This pattern is essential for transposon suppression (5), is established during early development and is maintained during DNA replication through interactions between proteins at the replication fork. Newly synthesized DNA is unmethylated and the hemimethylated structure of DNA that is generated during replication is recognized by Ubiquitin-like, containing PHD and RING finger domains, 1 (UHRF1) which, through a base flipping mechanism (6–9), allows DNA methyltransferase 1 (DNMT1) to access and methylate cytosines on the daughter strand (10–12). Both proteins are anchored to the DNA replication fork (13,14) through interactions with PCNA (12), LIG (15) and modified histones (12,16,17). In a cell free extract system, Uhrf1 was shown to load onto chromatin prior to origin licensing and to be required for origin replication complex (ORC) binding and

Received: August 7, 2023. **Revised:** December 12, 2023. **Editorial Decision:** December 31, 2023. **Accepted:** January 16, 2024
© The Author(s) 2024. Published by Oxford University Press on behalf of Nucleic Acids Research.
This is an Open Access article distributed under the terms of the Creative Commons Attribution-NonCommercial License (http://creativecommons.org/licenses/by-nc/4.0/), which permits non-commercial re-use, distribution, and reproduction in any medium, provided the original work is properly cited. For commercial re-use, please contact journals.permissions@oup.com

origin firing (18). Thus, the colocalization and coactivity of the methylation and replication factors assures faithful propagation of methylation patterns from parent to daughter cells and can coordinate these two processes.

The factors essential for DNA replication and maintenance DNA methylation are able to act together because their expression is co-regulated. UHRF1, DNMT1 and all of the genes required for DNA replication are targets of the E2F family of transcription factors (19–23). E2F is activated when retinoblastoma (Rb1) becomes phosphorylated by the cyclin-dependent kinases 4/6 (CDK)-Cyclin D complex which drives cells from G1 into S-phase. Therefore, the downstream consequence of CDK4/6 activation in response to mitogen stimulation assures that the factors required for both DNA replication and DNA methylation are present as cells enter S-phase. This coupling is essential, as in both during development and in cancer cells, inactivation of either UHRF1 or DNMT1 blocks cell proliferation (24–32).

Just as cell cycle regulatory pathways can regulate DNA methylation, the chromatin landscape can influence the cell cycle. For instance, repressive epigenetic marks restrict accessibility of E2F to it's target genes, and removal of repressive marks is essential for E2F function (33). The redistribution of repressive epigenetic marks during malignant transformation in many cell types leads to repression of the tumor suppressor, Cdkn2a (i.e. p16INK^{4a}), and thereby alleviates it's repression of Cdk4/6, and provides a constitutive signal to enter S-phase (34). A causative relationship between DNA methylation machinery and DNA replication was demonstrated by the finding that DNMT1/DNMT3B deficient cells have randomized replication timing (35). These examples demonstrate the complexity of the interplay between the ubiquitous cell cycle machinery and epigenetic modifiers to ensure fidelity of the epigenetic patterns as cells proliferate. Most studies linking epigenetic changes to the cell cycle are carried out in the context of cancer or using *in vitro* models, and it is not known whether similar mechanisms are at play during the rapid cell cycles that take place during vertebrate development.

The developing liver provides an optimal model to study this relationship, as liver outgrowth is mediated by proliferation of differentiated hepatocytes. In zebrafish, hepatocytes are specified and determined during the organogenesis stage of development (between 24–48 hpf) (36,37) and the differentiated hepatocytes proliferate while the liver undergoes morphogenesis during hepatic outgrowth. This stage is largely complete by 120 hpf (38). A few studies indicate that the mechanisms of cell cycle regulation during hepatic outgrowth utilize the same signaling pathways that control proliferation in most other cell types. For instance, genetic approaches in mice showed that E2F regulates hepatocyte proliferation during liver development and regeneration (39,40) and that hepatocyte specific knockout of Rb1 is sufficient to promote cell cycle entry, increased ploidy and generated large nuclei in postnatal and adult mouse hepatocytes (41,42). We discovered a functional relationship between *uhrf1* and cell cycle progression during hepatic outgrowth in zebrafish. *uhrf1* mutant embryos have multiple developmental abnormalities, including small head, defective gut, defective jaw, and a properly patterned liver that fails to grow (26,29,43). These phenotypes are first evident between 80–96 hours post fertilization (hpf) and are exaggerated at 120 hpf, resulting in lethality by 10 days post fertilization (dpf) (28). The cellular phenotypes of *uhrf1* deficient hepatocytes are similar to those of *dnmt1* mutants: both have large, misshapen nuclei, near complete loss of nuclear structures (44), and widespread cell death (26,28), which is dependent on Tnfa (45). Paradoxically, at 120 hpf, when DNA replication is complete in wild-type larvae (WT), nearly half of all *uhrf1* mutant hepatocytes continue to replicate their DNA and mutants have a gene expression signature typical for proliferating cells (28) but the liver fails to grow. The size of *uhrf1* mutant hepatocyte nuclei is nearly double that of controls (44), a phenotype that reflects increased ploidy (46). From this, we conclude that *uhrf1* mutant hepatocytes are arrested in S-phase, and undergo DNA rereplication. As in all other systems studied (10,11,29,47,48), *uhrf1* and *dnmt1* deficient zebrafish have DNA hypomethylation, which unleashes transposons that act as viral mimetics and trigger an interferon response (45,49). The mechanisms that contributes to the cell cycle defects in *uhrf1* mutants is not known and, more broadly how DNA methylation causes developmental defects also remains unclear.

Here, we reconcile the paradoxical observation that *uhrf1* zebrafish mutants a cellular and molecular phenotype associated with increased DNA replication and cell proliferation but the liver fails to grow. We identify Cdk4/6 activity as the mechanism giving rise to most of the developmental and cellular defects in *uhrf1* mutants, except for DNA hypomethylation, transposon activation and induction of the interferon response. The Cdk4/6 inhibitor, Palbociclib, rescues all embryonic morphological defects in *uhrf1* mutants, including liver size, DNA replication, nuclear enlargement, cell death and larval survival. Cdk4/6 signaling is also activated in *dnmt1* mutants, and both mutants show cases, the Cdk4/6 inhibitor suggesting that DNA hypomethylation as the underlying mechanism. Since DNA replication does not occur in *dnmt1* mutants and Dnmt1 depletion in *uhrf1* mutant hepatocytes blocks DNA replication, we concluded that Dnmt1 is essential at the replication fork (13,14). *uhrf1* mutants have replication stress and DNA damage, which induces the Ataxia Telangiectasia And Rad3 Related (Atr) pathway, and we show that DNA replication and the small liver size in *uhrf1* mutants in part requires Atr signaling. These data provide new mechanistic insight into the interaction between key cell cycle regulatory pathways and DNA methylation during development, indicate the importance of the Cdk4/6 pathway as mediating the cellular consequences of Uhrf1 depletion. This also suggests that the important chemotherapeutic, Palbociclib, may modulate the cellular response to epigenetic defects.

Materials and methods

Biological resources

Adult zebrafish were maintained in a circulating aquaculture system on a 14:10 hours light: dark cycle at 28°C. The *uhrf1*^{hi272} allele (50) was maintained by genotyping adults by PCR to identify heterozygous carriers as described (26). Homozygous mutant embryos were generated by crossing heterozygous adults and were identified based on distinctive phenotypes as described (26,28,29) or by genotyping individual embryos as described (26). *Tg(fabp10a: nls-mCherry)*;*uhrf1*$^{hi272+/-}$ and *Tg(fabp10a: CAAX-EGFP)*;*uhrf1*$^{hi272+/-}$ were used for all experiments to enable liver detection (51). Homozygous *uhrf1*$^{hi272-/-}$mutant larvae are hereafter called *uhrf1*$^{-/-}$. Ho-

mozygous *dnmt1*$^{s904-/-}$ mutants (*dnmt1*$^{-/-}$) were generated by crossing *dnmt1*$^{s904+/-}$ adults in *dnmt1*$^{s904+/-}$*;Tg(c269*^{off}*; 10XUAS:dsRed); (fabp10a:Gal4; cmlc2:EGFP)* background to monitor DNA methylation in the liver as described (45). All protocols were approved by the NYU Abu Dhabi Institutional Animal Care and Use Committee (IACUC; protocol # for zebrafish: 22–0003A3).

Mice maintenance and experiments were approved by the New York University Abu Dhabi IACUC (protocol # for mice: 20_0006A4). Temperature, humidity, and light:dark cycles were controlled and mice were fed standard chow and water *ad libitum*. C57BL/6 mice with hepatocyte-specific deletion of the Uhrf1 gene (*Uhrf1*$^{fl/fl}$*;Alb-Cre*; referred to as *Uhrf1*^{HepKO} mice) were generated by crossing mice homozygous for floxed *Uhrf1* (*Uhrf1*$^{fl/fl}$) with mice expressing the Cre recombinase under the liver-specific albumin promoter back- crossed onto the *Uhrf1*$^{fl/fl}$ background (*Alb-Cre*$^{Tg/+}$*; Uhrf1*$^{fl/+}$) as described previously (48). P4 mice were sacrificed and their livers were collected, flash frozen in liquid nitrogen, and stored at -80°C then processed for RNA extraction.

CRISPR/Cas9 generation and T7 endonuclease assay

sgRNAs for *dnmt1* were designed using ChopChop (https://chopchop.cbu.uib.no/) and were co-injected with the control sgRNA targeting the *slc45a2* gene, which is involved in pigmentation to enable sorting of efficiently targeted embryos (43,52). Genotyping primers were designed by Primer3 (https://bioinfo.ut.ee/primer3-0.4.0/) and validated in USCS Genome Browser (https://genome.ucsc.edu/cgi-bin/hgPcr). The sgRNA and primer sequences are provided in Supplementary Table S1. sgRNAs were produced by sgRNA IVT kit (Takara Bio) by following the manufacturer's instructions and RNA was isolated by Trizol (Invitrogen). sgRNAs were quantified by Qubit RNA BR kit and diluted at 50 ng/μl and stored as single use aliquots. The efficiency of the sgRNAs were assessed by injecting all 4 *dnmt1* sgRNAs into WT embryos with equal volume of previously diluted nls-Cas9 protein (IDT; 0.5 μl of nls-Cas9 added with 9.5 μl of 20 mM HEPES; 150 mM KCl, pH 7.5) and sgRNAs, incubated at 37°C for 5 min and then 1 nl was injected in 1–2 cells stage embryos. At 24–72 hpf, 12–16 sgRNA injected embryos were individually collected and genomic DNA was extracted by heat shock denaturation in 50 mM NaOH (95°C for 20 min). For each embryo, PCR was performed on genomic DNA by using Q5 High-Fidelity Taq Polymerase (New England Biolabs) followed by T7 endonuclease I assay (New England Biolabs) to detect indel mutations. For T7 endonuclease I assay, 10 μl of PCR product was incubated with 0.5 μl of T7e1 enzyme (New England Biolabs) for 30 min at 37°C. Digested and undigested fragments were run in parallel in 2% agarose gel to assess the presence of indels. Efficiency was calculated as the number of embryos that show a positive result based on T7e1 assay divided by the total number of embryos assayed for the sgRNAs. Once established for efficiency, the pool of 4 *dnmt1* sgRNAs were injected into the 1 cell embryos generated by an incross of *uhrf1*$^{+/-}$ adults as previously described. Uninjected embryos or slc45a2 crispants were used as control. The resulting F_0 larvae were considered crispants. For each clutch, *uhrf1*−/−mutants were divided from phenotypically WT siblings at 5 dpf based on morphological differences and T7e1 assay. sgRNA sequence information and genotyping primers are provided in Supplementary Table S1.

Chemical treatment

The CDK4/6 inhibitor Palbociclib (PD-0332991, Sigma Aldrich) (53) was dissolved in DMSO (Sigma) to yield a 10 mM stock solution and stored at −80°C. Palbociclib was dissolved in 0.5% DMSO embryo water at a concentration of 20 μM and added to 48 hpf dechorionated embryos in 6 well plates; siblings that were treated with 0.5% DMSO were used as controls and collected at indicated timepoints. The ATR inhibitor VE-821 (ab219506, Abcam) (54) was dissolved in DMSO (Sigma) to yield a 20 mM stock solution and stored at −20°C. For the *in vivo experiments*, VE- 821 was dissolved in embryo water at a concentration of 10 μM and added to 48 hpf dechorionated embryos; DMSO (1:2000 dilution) in embryo water was used as a control. To induce DNA damage, 120 hpf control embryos were treated in 0.25% H_2O_2 (Sigma Aldrich) for 30 min and processed either for EdU incorporation or for western blot.

Survival assay

Heterozygous *uhrf1*$^{bi272+/-}$; *Tg(fabp10a: nls-mCherry)* $^{+/-}$ adults were incrossed and split into 40 embryos per 90 mm Petri plate, with around 25% *uhrf1*$^{-/-}$ per plate. The embryos were dechorionated and treated with either 0.5% DMSO or 20 μm Palbociclib at 48 hpf. At 120 hpf, the larvae were transferred to fresh embryo water and monitored until 9 dpf, individually collected and genotyped.

Protein lysates and western blotting

For western blots, whole larvae from *uhrf1*$^{-/-}$ and control siblings were collected at 120 hpf in RIPA buffer (10 mM Tris–HCl pH 8.0, 1 mM EDTA, 0.5mM EGTA, 1% Triton X-100, 0.1% sodium deoxycholate, 0.1% SDS, 140 mM NaCl supplemented with protease inhibitor cocktail (Machery-Nagel), sonicated using a hand sonicator (Hielscher Ultrasonics), and centrifuged at 14 000 g for 15 min at 4°C to remove cell debris. Supernatant was collected and SDS-PAGE loading Leammli buffer (BioRad) was added and run on SDS-PAGE gel. Volume corresponding to 4–5 larvae was loaded on 10–12.5% acrylamide gels, transferred onto PVDF membranes, blocked with 5% w/v Bovine Serum Albumin (Sigma) in TBST (20 mM Tris–HCl, 150 mM NaCl, 0.1% v/v Tween 20, pH 8.0) for 1 h at room temperature and incubated overnight in primary antibody (1:1000 Chk1(S345) (Cell Signaling Technologies), 1:1000 anti-Phospho-RPA32 (S33) (Abcam), 1:1000 H2AX (S139) (Genetex), 1:1000 1:1000 H3 polyclonal (Santa Cruz) diluted in blocking buffer at 4°C. The following day membranes were washed 3 times in TBST for 5 min and incubated in secondary antibody (1:2500 anti-rabbit or anti-mouse HRP-conjugated, Promega) diluted in blocking buffer for 1 h at room temperature and washed 3 times with TBST for 5 min at room temperature. Chemiluminescent signals using Pierce™ ECL Western Blotting Substrate (Thermo Fisher Scientific) or Clarity ECL substrate (BioRad) and imaged using Bio-Rad ChemiDoc. Immunoblot bands are quantified by densitometry using GelAnalyzer (http://www.gelanalyzer.com) and plotted using GraphPad Prism 9. 3 independent clutches were used for quantification. Levels of were normalized to the level of H3 for each sample.

RNA and DNA extraction

For each clutch, 10 to 20 livers were microdissected from either *dnmt1*$^{-/-}$ or *uhrf1*$^{-/-}$ and their phenotypically normal siblings in *Tg(fabp10a: CAAX-EGFP)* background larvae to facilitate liver identification as described (55). RNA was extracted using Trizol (Invitrogen) following the manufacturer's instructions with modifications. Briefly, during precipitation in isopropanol, 10 μg of Glycoblue (Thermo Fisher Scientific) was added, and precipitation performed overnight at −20°C followed by 1 h centrifugation at 12 000 g at 4°C. The resultant RNA pellet was resuspended in water and quantified by Qubit RNA High Sensitivity kit (Thermo Fisher). For genomic DNA extraction, each embryo was subjected to DNA extraction buffer (10 mM Tris–HCl pH9, 10 mM EDTA, 200 mM NaCl, 0.5% SDS, 200 μg/ml proteinase K) followed by DNA precipitation with isopropanol as described (49). DNA was resuspended in water and quantified by Qubit dsDNA High Sensitivity kit (Thermo Fisher).

Slot blot analysis

Slot blot was performed as previously described (28). Briefly, 2 ng of genomic DNA was denatured in 400 mM NaOH/10 mM EDTA and each sample was blotted onto nitrocellulose membrane in duplicate in the slot blot apparatus, with one replicate probed for dsDNA and the other for 5-methylcytosine (5-MeC). Membranes were incubated 1 h at 80°C, blocked with 5% skim milk in TBST (37 mM NaCl, 20 mM Tris pH 7.5, 0.1% Tween 20), and incubated overnight at 4°C in either anti-dsDNA (Abcam, 1:8000 in 2% BSA in TBST) or 5-meC (Aviva Biosystem clone 33D3, 1:2000 in 2% BSA in TBST). Membranes were washed in TBST and probed with anti-mouse HRP secondary antibody (Promega; 1:5000 in 2% BSA in TBST) for 1 hour at room temperature followed by development in ECL (Thermo Fisher Scientific). ChemiDoc (Bio-Rad) was used to detect and quantify the chemiluminescent signal. Samples from seven clutches were analyzed using the GelAnalyzer (http://www.gelanalyzer.com) to measure the signals and ratio between 5-MeC and dsDNA was plotted for controls and mutants in each clutch using GraphPad Prism 9.

cDNA production and qPCR

RNA extracted from microdissected liver was retrotranscribed to cDNA using Qscript cDNA synthesis kit (Quanta Bio) following the manufacturer's instructions. cDNA was diluted to 1 ng/μl, and 5 μl was used per reaction for qPCR using Maxima R SYBR green/ROX master mix (Thermo Fisher Scientific). *rplp0* (in zebrafish) and *Gapdh* (in mice) were used to normalize expression levels by using the calculations for delta-Ct, and control siblings were used to calculate delta-delta-Ct (DDCt) as previously described (56). To determine changes in expression between control and experimental samples, the fold change was calculated and expressed as the $\log_2$ value (L2FC) for display. All experiments were performed on samples from at least two independent clutches, with the number of biological replicates indicated for each experiment. Primers information is provided in Supplementary Table S1.

Left lobe liver size and cell number measurements

Liver size measurements were carried out based on the 2D area of the left liver lobe in 120 hpf larvae. Embryos from cross of *Tg(fabp10a: nls-mCherry)* in *uhrf1*$^{+/-}$ and *Tg(fabp10a: CAAX-EGFP)* in *uhrf1*$^{+/-}$ background was used for all experiments for ease of liver detection. The live embryos were mounted in 3% methylcellulose on the right side and the left liver lobe was imaged using Nikon Elements on a Nikon SMZ25 Stereoscope. Liver size measurements were calculated in ImageJ using free hand selection of the EFGP/ cherry labeled area corresponding to the left liver lobe, and analyzed using the shape descriptor sub-function to determine the area of the left liver lobe, expressed in μM^2. For Palbociclib treatment, *uhrf1*$^{-/-}$ liver size of 20000 μM^2 and below was considered small liver phenotype and *uhrf1*$^{-/-}$ liver size above 20 000 μM^2 considered as rescued. For cell number measurements, embryos from incross of *Tg(fabp10a: nls-mCherry);uhrf1*$^{+/-}$ were fixed in 4% PFA for 2 h at room temperature and washed with PBS. Embryos were mounted in 1% low melting agarose and Z-stacks of of the whole liver were acquired with Leica Stellaris Confocal Microscope. nls-mCherry positive nuclei were counted using the interactive 3D measurement tool in LASX. Z-stacks were compiled into a 3D image, were adjusted for threshold and noise and a minimum size of 100 voxels was set to define the nuclei. For each condition, at least three livers were analyzed.

Immunofluorescence

120 hpf control siblings and *uhrf1*$^{-/-}$ zebrafish embryos containing the *Tg(fabp10a: nls-mCherry)* transgene to identify hepatocyte nuclei were fixed in 4% paraformaldehyde for 4 h at room temperature, washed in PBS, and treated with 150 mM Tris–HCl at pH 9.0 for 5 min, followed by heating at 70°C for 15 min according to an established protocol (57) and following incubation at room temperature to cool the embryos and washed in PBS. Livers were dissected as described, permeabilized with 10 μg/ml Proteinase K (Macherey-Nagel) in PBS containing 0.1% tween (PBST) for 10 min, washed 3 times with PBS, and incubated in a blocking solution containing 5% fetal bovine serum (GIBCO) in PBS for 60 min at room temperature. The blocking solution was removed, and the livers were then incubated in 100 μl of Cdkn2a/b sc-1661, SantaCruz), Phospho RPA32 (S33) (ab211877), or H2AX (phospho S139) (GTX127342, GeneTex Inc.) primary antibody in blocking solution (1:200 dilution) overnight at 4°C. After 3 washes in PBST, the livers were incubated in secondary antibody (Molecular Probes) in blocking solution (1:400 dilution) in the dark for 2 h on a shaker. After 5 washes with PBST, the nuclei were counterstained with Hoechst (Thermo Fisher Scientific) diluted 1:1000 in PBS, washed twice with PBS to remove excess Hoechst, and mounted on a microscope slide with Vectashield (Vector Laboratories) and covered with a 0.1 mM coverslip for imaging using Leica SP8 confocal microscope.

Terminal deoxynucleotidyl transferase dUTP nick end labeling assay (TUNEL)

Larvae collected at 5 dpf were fixed in 4% paraformaldehyde for 4 h at room temperature, and gradually dehydrated through a graded series of methanol and stored in 100% methanol at 4°C overnight. Gradual rehydration to PBS through a graded series of methanol/PBS dilutions was carried out at room temperature. Larvae were permeabilized with 10 μg/ml Proteinase K (Macherey-Nagel) in PBS containing 0.1% tween (PBST) and fixed in 4% Paraformaldehyde for 10 min at room temperature. Livers were then dissected and

subjected to TUNEL assay according to manufacturer's instructions (*In Situ* Cell Death Detection kit, Fluorescein; Roche). Nuclei were counterstained with Hoechst (Thermo Fisher Scientific) diluted 1:1000 in PBS, mounted on a microscope slide with Vectashield (Vector Laboratories) and covered with a 0.1 mM coverslip for imaging using Leica SP8 confocal microscope.

EdU incorporation for S-phase analysis

Ten live larvae at 80 hpf, 96 hpf or 120 hpf were transferred into 50 ml falcon tube with 250 µl solution 1 mM EdU (ThermoFisher) in 10% DMSO in embryo water, and incubated on ice for 20 min. Room temperature embryo water was added to 50 ml, and embryos were further incubated for either 12 min or 30 min at 28.5°C. After removing the embryo water, the embryos were fixed in 4% paraformaldehyde (Electron Microscopy Sciences) overnight at 4°C, then dehydrated through a graded series of methanol and incubated in 100% methanol overnight at 4°C and gradually rehydrated back to PBS by serial dilutions of methanol. The embryos were then permeabilized with 10 µg/ml Proteinase K (Macherey-Nagel) in PBST for 15 min prior to the Click-iT reaction to attach the Alexa azide (Invitrogen). The larvae were transferred to a solution of 172 µl PBS, 8 µl CuSO4 (100 mM), and 0.2 µl Alexa azide in a 0.6 µl microcentrifuge tube, and rocked in the dark for 10 min. 20 µl of ascorbic acid (0.5 M) was added, and the samples were rocked in the dark for additional 20 min. Then the mixture was removed and a fresh Alexa azide solution was added, and the same steps were repeated once more. 80 hpf embryos were individually genotyped by collecting tail samples. The larvae were washed 4 times in PBST prior to dissection and mounted in Vectashield mounting medium with DAPI before they were imaged with the Leica SP8 confocal microscope.

Confocal imaging, image processing and analysis

Confocal imaging was performed using Leica TCS SP8 microscope with a 40x oil immersion at a scan speed of 100 Hz. For antibody immunofluorescence stains and TUNEL experiments, images were acquired at different focal distances from each liver and LAS X software (Leica software) was used for quantification from three separate optical sections per liver, which were then averaged from three livers per clutch per condition, and a minimum of two clutches were analyzed for every condition. For EdU and nuclear morphology measurements, Z-stacks were acquired using the galvo stage, with 2 µm intervals. Bit depth was 12, and to enhance image quality, field of view and laser intensity were adjusted separately for each sample. The acquired images were visualized using LASX software. 3D analysis of Z-stacks of Hoechst-stained nuclei was performed using the interactive 3D measurement tool in LASX for volume, surface area, sphericity, elliptical mean, and nuclei counting with DAPI and EdU stains. Z-stacks were compiled into a 3D image, were adjusted for threshold and noise to define the nuclei clearly, set for minimum size to be measured as 100 voxels, and measurements of the previously mentioned parameters obtained and exported in excel spreadsheets. For each time point and parameter measured, no less than 100 nuclei were sampled from at least three livers per condition. Results were plotted in GraphPad Prism 9. Intensity measurements were analyzed on 2D sections with ImageJ using published methods (58). To calculate the co-localization between γH2AX and EdU staining, an automatedapproach was used to measure colocalization using ImageJ (Pearson's *R* value, JACoP plugin, ImageJ) using published methods (59,60).

RNA-Seq

Fifty livers were dissected at 120 hpf from Palbociclib or DMSO treated control sibling or *uhrf1*$^{-/-}$; *Tg(fabp10a:CAAX-EGFP)* larvae as previously described. The livers were individually collected and stored at -80°C while the carcasses were genotyped for *uhrf1* mutation (26). Once genotyped, the *uhrf1*$^{-/-}$ livers and control livers from each individual clutch were pooled and RNA extracted according to established protocols (45). 100 ng of RNA was used for library preparation according to the manufacturer's instructions (Illumina, San Diego, CA, USA). Libraries were sequenced on NovaSeq (Illumina) to obtain 150 bp paired-end reads. Raw Fastq files quality was assessed by using FASTQC and the reads were quality trimmed using Trimmomatic (61) to remove low quality reads and adapters. Qualified reads were mapped to the reference genome Danio rerio GRCz10. To estimate and compare gene expression in different data sets, raw reads were uploaded to http://tsar.abudhabi.nyu.edu/ for pre-processing and DeSeq2 for Differential gene expression analysis. Datasets of RNAseq performed on 120 hpf *uhrf1*$^{-/-}$ and *dnmt1*$^{-/-}$ and their controls is previously published (45) and available at GEO (GSE160728). Dataset of RNAseq performed on 120 hpf *uhrf1*$^{-/-}$ and sibling controls treated with Palbociclib or DMSO are available on GEO (GSE234993).

Bioinformatic analysis

For Gene Ontology and Ingenuity Pathways Analysis (IPA) zebrafish gene names were converted into human gene names using Biomart. Differentially expressed genes were determined by *P*-value adjusted <0.05 and $\log_2$ fold change 0. GO enrichment analysis of differential expressed genes was conducted using REVIGO (62) to find enriched terms for different DEG data sets. An adjusted *P*-value <0.05 was considered significant for all analyses. UPSET plots were generated to show intersections of enriched terms from REVIGO, their size and unique terms (63). Heatmaps were generated with Pheatmap on z-score of normalized counts. For plotting and statistical analysis, R package 'ggplot' and GraphPad Prism 9 software were used.

Statistical analysis

All experiments were carried out on multiple larvae from at least two clutches, with exact numbers of animals and clutches indicated in each figure legend. Data represented as the median with the range and, where appropriate, individual sample measurements are plotted. The unpaired two-sided student *t* test was employed to compare the medians between groups with adjustment for multiple comparisons. One exception was the liver size segregation where mean with SD was plotted. All of the data were considered to be significant at $^{*}P < 0.05$, $^{**}P < 0.005$, $^{***}P < 0.0005$. All plots along with statistical analysis were generated in GraphPad Prism 9 (GraphPad Software). Bioinformatic analysis and visualization of genomic data were performed and plotted in RStudio.

Reagents

Enzymes: Proteinase K (740396, Machery-Nagel, Germany), Q5 Hot Start High-Fidelity DNA Polymerase (M0493S, New England Biolabs, USA), DNase I (EN0521, Thermo Fisher, UAE), T7 Endonuclease I (M0302S, New England Biolabs, USA).

Antibodies and stains: Primary antibodies- Cdkn2a/b (sc-1661, SantaCruz, USA), Phospho RPA32 (S33) (ab211877, USA), H2AX (phospho S139) (GTX127342, GeneTex Inc, USA.), Chk1 (phospho S345) Clone 133D3 (2348P, Cell Signaling Technology), H3 (sc-10809, SantaCruz, USA). Secondary antibodies (A21202, A21422, A11010, A21245, Molecular Probes, USA), HRP-conjugated antibodies (W4021, W4011, Promega). Click-IT reagents: Alexa Fluor 647 Azide, Triethylammonium Salt (A10277, Invitrogen, USA), Alexa Fluor 488 Azide, Triethylammonium Salt (A10266, Invitrogen, USA), EdU (A10044, Thermo Fisher, UAE). Hoechst (62249, Thermo Fisher, UAE), Vectashield (H1000, Vector Laboratories, USA).

Kits: Guide-it sgRNA In Vitro Transcription Kit (632635, Takara, Japan), Qubit RNA BR kit (Q10210, Invitrogen, USA), Trizol (15596026, Thermo Fisher, UAE), qScript cDNA synthesis kit (95047, Quanta Bio, USA).

Results

DNA replication is a primary cellular response to *uhrf1* loss

We previously reported that *uhrf1* mutant livers have an increased number of cells that incorporate nucleotides during hepatic outgrowth, that the nuclei are large, and that nucleotide incorporation continues over several days during development, despite the livers being smaller sized (28), suggesting DNA rereplication or aberrant origin firing. To identify when this defect first occurred during hepatic outgrowth, we pulsed embryos at 80, 96 and 120 hpf for 30 min with EdU, sorted *uhrf1* mutants based on morphological phenotypes at 96 hpf and 120 hpf, and, since the phenotype is not apparent at 80 hpf, all embryos at this time point were individually genotyped. All embryos were assessed for the number of hepatocytes with EdU incorporation. Nearly all hepatocytes in *uhrf1* mutants and their phenotypically normal siblings (heretofore referred to as controls) were EdU positive at 80 hpf. At 96, and 120 hours, EdU positive hepatocytes were reduced to 25% and 10%, respectively in control larvae, while 55% and 43% of *uhrf1* mutant hepatocytes were EdU positive at these same time points (Figure 1A, B).

The stereotypical pattern of DNA replication has euchromatic DNA replicated in early S-phase, visualized as homogeneous EdU labeling in the nucleoplasm, followed by replication of DNA in the nuclear lamina during mid-S-phase and heterochromatin replicated last (64). If the increase in EdU incorporation in *uhrf1* mutant hepatocytes reflected DNA replication, then these patterns should be apparent. Scoring S-phase stage based on the patterns of EdU incorporation showed that at 80 hpf, most hepatocytes in controls and *uhrf1* mutants were in early S-phase, while at 96 hpf and 120 hpf there was a significant increase in the number of *uhrf1*$^{-/-}$ hepatocytes in mid and late S-phase, respectively (Figure 1C). These data rule out the possibility that EdU incorporation in *uhrf1* mutant hepatocytes reflects DNA damage repair, as repair mediated nucleotide incorporation does not mirror the stereotypical stages of DNA replication (65,66). Interestingly, we observed that *uhrf1*$^{-/-}$ hepatocytes incorporate EdU in a pattern that reflects a pattern of heterochromatin and intact nuclear lamina even though these hepatocytes are devoid of the nuclear lamina marker Lamin A (44).

We hypothesized that the EdU incorporation phenotype in *uhrf1* mutant hepatocytes reflected either an acceleration of the fork progression rate or an increase in the number of active origins. To test this, we optimized the duration of the EdU pulse to be just below the limit of detection in control hepatocytes at 120 hpf (Supplementary Figure S1). Following a 12 min pulse with EdU, no hepatocytes were labeled at either 80 or 120 hpf in control larvae or in *uhrf1*$^{-/-}$ larvae but nearly 40% of *uhrf1* mutant hepatocytes were labeled at 120 hpf (Figures 1D and Supplementary Figure S1). Most of the cells that incorporated EdU during this short pulse had a pattern that reflected early S-phase, (Figure 1D), suggesting that Uhrf1 deficiency either induces firing of more DNA replication origins or increases replication fork speed.

CDK4/6 is activated in *uhrf1* mutant livers

To identify the basis of the DNA replication defect, we analyzed bulk RNAseq data from pools of control and *uhrf1* mutant livers collected at 120 hpf (45), when the hepatic developmental and cellular phenotypes are fully penetrant. Gene ontology (GO) analysis using REVIGO revealed that downregulated genes were mainly involved in hepatic functions, such as protein modification and lysis, signaling and metabolic process, while the upregulated genes were enriched in pathways involved in cell cycle regulation, DNA replication, anti-viral and immune response and cell death (Figure 2A, Supplementary Table S2). UPSET analysis of the differentially expressed genes (DEGs) in all of the cell cycle pathways identified by REVIGO demonstrated that many genes were common to multiple genesets, however a cluster of genes involved in DNA replication and cell division were unique (Figure 2B; Supplementary Table S2). These data confirm and extend our previous findings (26,28,45) that *uhrf1* mutant livers have aberrant cell cycle regulation.

We next used Ingenuity Pathway Analysis (IPA) of the unified set of all DEGs in the GO term genesets related to the cell cycle to identify potential upstream regulators of the cell cycle DEGs in *uhrf1* mutant livers. This uncovered a pattern whereby the G1/S and G2/M checkpoint pathways were downregulated and cell cycle regulation, proliferation and transition through the cell cycle were upregulated (Figure 2C, Supplementary Table S3). The key upstream regulators of the G1/S transition and S-phase entry and progression, *Cdk4/6-Cyclin D, Cdk2-Cyclin E* and the DNA replication initiation factor, *Cdc25a*, were upregulated in *uhrf1* mutant livers. Additionally, the cell cycle inhibitor *cdkn1b* and the cell cycle regulated gene *rbl2*, which prevents access of E2F1 and is a UHRF1 interacting protein (67), were downregulated (Figure 2D). Interestingly, this analysis uncovered DNA damage responses to be induced, with *atr* upregulation as a leading gene implicated in several the pathways. It also showed that the cell cycle inhibitor Cdkn2c is highly expressed in *uhrf1* mutant livers, suggesting that both pro- and anti-proliferative signals are simultaneously activated in *uhrf1* deficient hepatocytes. Together, these data suggest that loss of *uhrf1* results in repression of G1/S and G2/M cell cycle checkpoints, activation of Cdk4/6 and its downstream targets. It also suggests activa-

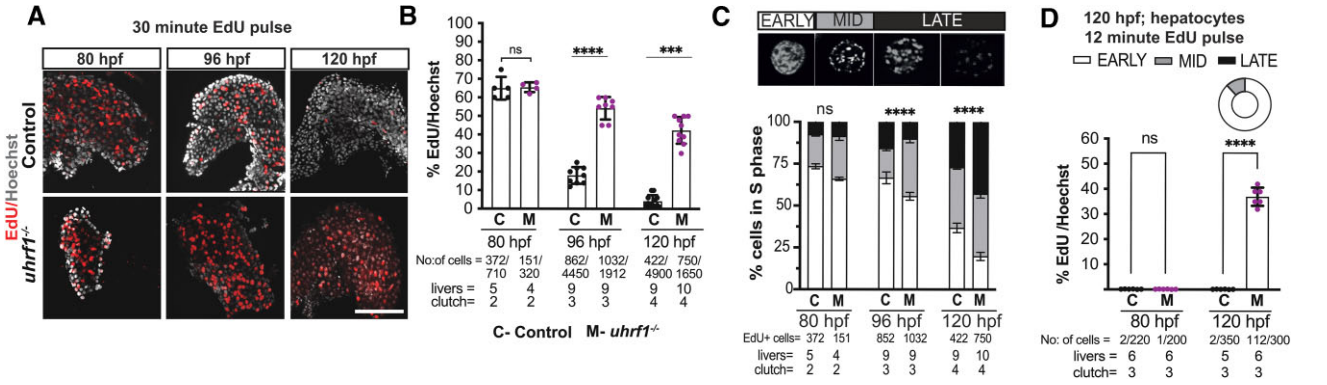

Figure 1. *uhrf1* mutant hepatocytes accumulate in late S-phase with increased DNA replication. (**A**) Representative Z-stack projection confocal images of EdU and Hoechst stained control and *uhrf1*$^{-/-}$ livers. Control and *uhrf1*$^{-/-}$ embryos were pulsed with EdU for 30 min at 80 hpf, 96 hpf and 120 hpf and processed for EdU fluorescence by Click-it. (**B**) Quantification of EdU incorporation in A. (**C**) 80 hpf, 96 hpf and 120 hpf hepatocytes were sorted into early, mid and late S phase based on EdU pattern and quantified. (**D**) Quantification of EdU incorporation from a 12 min EdU pulse at 80 hpf and 120 hpf control and *uhrf1*$^{-/-}$ hepatocytes. Pie chart represents percentage of hepatocytes in each stage of S phase. Scale bar = 50 μm, the number of samples and clutches indicated for each condition and represented as median with range. *P*-value *< 0.05, **< 0.005, *** < 0.0005 by unpaired Student's *t*-test with adjustment for multiple comparisons.

tion of other cell cycle checkpoints so that cells receive signals that both promote G1/S transition and DNA replication and prevent full cell cycle progression.

These data establish a developmental timeline of the *uhrf1* mutant hepatic phenotypes whereby DNA hypomethylation (45), and nuclear size defects are first detected at 80 hpf (44), followed by increased DNA replication (Figure 1A, B) and cell death at 96 and 120 hpf. Since no cell cycle DEGs were detected at 80 hpf (28) but qPCR analysis on RNA from pooled livers dissected at 96 hpf showed that several cell cycle regulatory genes (*ccne1, ccna2)*, replication licensing factors (*mdm2, mcm3, orc3, cdc6)* and processivity factors (*pola1, pold1* and *pcna*) were upregulated at this time point (Figure 2E), we generate a time course in which DNA hypomethylation occurs as a first consequence of Uhrf1 loss, followed by upregulation of Cdk4/6, increased DNA replication and cell death from 96 hpf onwards. Importantly, we found a similar effect on cell cycle genes in the liver of neonatal mice at P4 where the *Uhrf1* locus has been deleted by Cre (Figure 2F, inset) in hepatocytes ((Alb:Cre$^{Tg/+}$;Uhrf1$^{fl/f}$ i.e. *Uhrf1*^{HepKO}) (48). All cell cycle genes analyzed (except *Mcm6* were upregulated in *Uhrf1*^{HepKO} livers (Figure 2F, G). This suggests that Uhrf1 plays a conserved role in regulating the cell cycle during hepatic outgrowth.

Cdk4/6 activation is required for the *uhrf1* mutant phenotype

We hypothesized that Cdk4/6 and E2F activation combined with loss of G1/S checkpoints could drive Uhrf1 deficient cells into S-phase. To test this, we used the Cdk4/6 inhibitor Palbociclib (PD in figures), which is an approved chemotherapeutic for breast cancer (68) that effectively suppresses DNA replication and cell proliferation in liver cancer cells (53). We optimized the dose and timing of Palbociclib exposure to obtain the maximal tolerable administration dose to achieve no effects on control larvae based on survival, overall embryo phenotype, morphological criteria and liver size (Supplementary Table S4). The final treatment scheme outlined in Figure 3A involved adding 20 μM Palbociclib in 0.5% DMSO or 0.5% DMSO as a control to 48 hpf embryos generated from an incross of *uhrf1*$^{+/-}$ adults which expressed nuclear localized signal targeted cherry transgene in hepatocytes (*Tg(fabp10a: nls-mCherry)*) to mark the livers. The resulting larvae were collected at 120 hpf, imaged to assess morphological features characteristic of *uhrf1* mutants and then all larvae were individually genotyped.

At 120 hpf, *uhrf1* mutants are distinguished by smaller head, lower jaw deformity, microphthalmia, underdeveloped gut and small liver (Supplementary Figure S2A; (26,28)). These phenotypes are fully penetrant at 120 hpf, so that on average, 25% of embryos resulting from an incross of *uhrf1*$^{+/-}$ adults display all of these phenotypes (Supplementary Figure S2B). However, we found only 7% of embryos produced from an incross of *uhrf1*$^{+/-}$ adults treated with 20 μM Palbociclib have all mutant phenotypes while 18% of embryos showed a partial mutant phenotype, with restoration of the lower jaw defect, increase in liver size, or both (Supplementary Figure S2B, C). When these embryos were genotyped, we uncovered the expected genotype-phenotype relationship in 100% of embryos in DMSO treated clutches, so that all embryos displaying the mutant phenotypes were *uhrf1*$^{-/-}$ and all embryos that lacked these phenotypes were either WT or heterozygotes. However, in Palbociclib treated clutches, embryos with a partial phenotype and even a few scored as normal were homozygous mutants (*uhrf1*$^{-/-}$;Supplementary Figure S2C, D).

Palbociclib had no significant effect on liver size in WT embryos, but significantly increased the size of the liver (Figure 3B–D), the number of hepatocytes (Figure 3D) and eye size (Supplementary Figure S2E) in *uhrf1* mutants. The liver size of nearly all *uhrf1* mutants treated with Palbociclib exceeded the average liver size in DMSO treated mutants, and 20% of treated mutants had a liver size that was within the range of WT embryos (Figure 3C).

To differentiate aspects of the *uhrf1* mutant phenotype that were a direct consequence of Uhrf1 loss compared to those that were mediated by Cdk4/6 activation, we assessed the effects of Palbociclib on the cellular aspects of hepatic phenotypes: EdU incorporation, nuclear size and shape and cell death. These parameters were unchanged by Palbociclib treatment of control embryos, but were significantly rescued in *uhrf1* mutants. The number of hepatocytes with EdU incorporation at 120 hpf was reduced from 40% in untreated mutants to 28% in Palbociclib treated *uhrf1* mutants (Figure 3E).

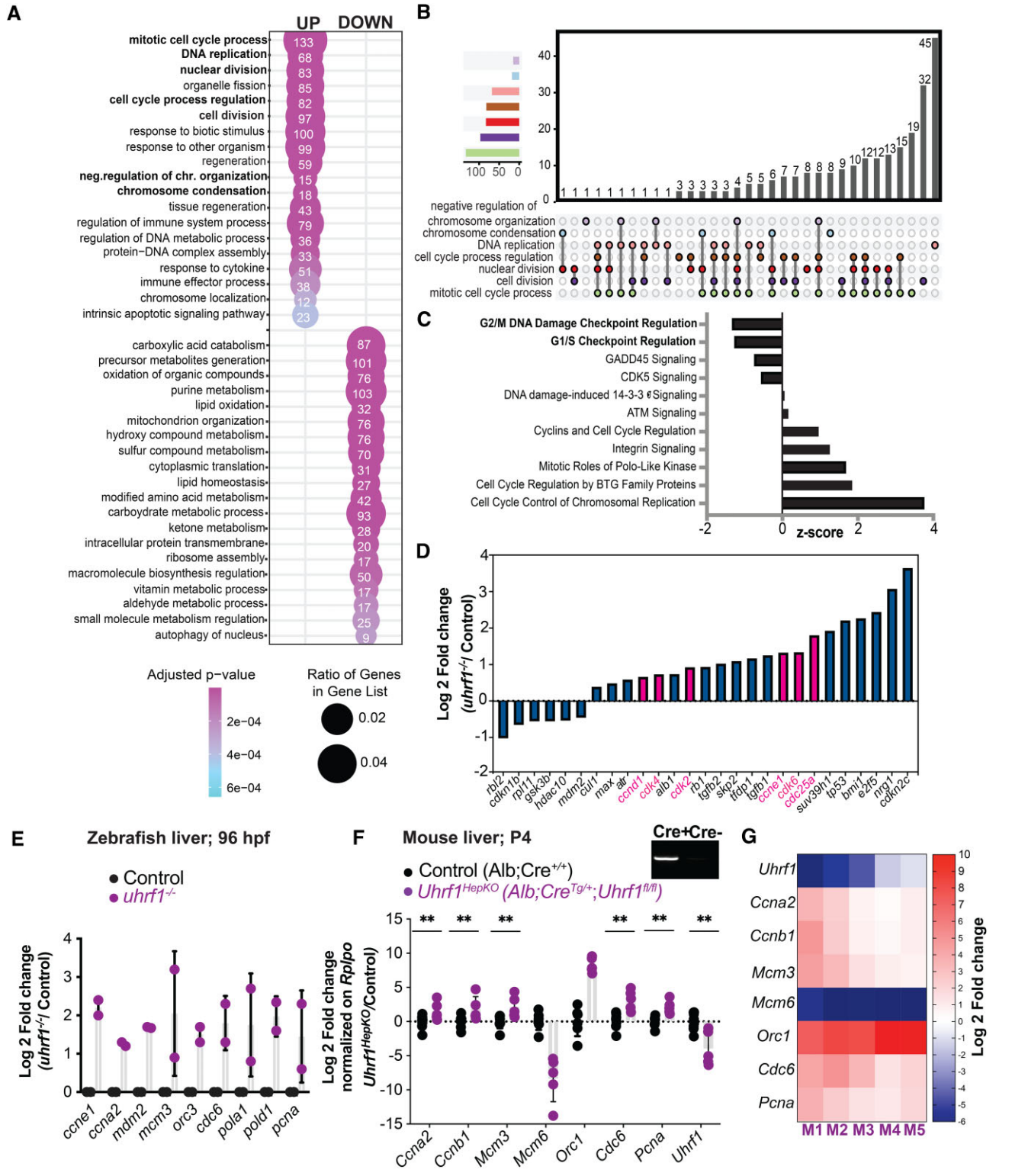

Figure 2. CDK4/6 is activated in *uhrf1* mutant livers. (**A**) Gene ontology (REVIGO) of the significant upregulated and downregulated genes in 120 hpf *uhrf1*$^{-/-}$ liver RNA-Seq (*P*-adj < 0.05) for each category. The cell cycle GO terms are highlighted in bold. (**B**) UPSET plot of all the cell cycle GO category genes from A. (**C**) Ingenuity Pathway Analysis (IPA) of all the cell cycle genes differentially expressed in 120 hpf *uhrf1*$^{-/-}$ liver RNA-Seq, pathways involved in cell cycle checkpoint regulation in bold, z- score in IPA indicates a predicted activation or inhibition of a pathway. (**D**) Genes from the G1/S checkpoint pathway generated by IPA plotted with log2fold change, important cell cycle genes highlighted in red. (**E**) qPCR on key cell cycle genes of 96 hpf *uhrf1*$^{-/-}$ and control livers. (**F**) qPCR on key cell cycle genes in the livers of P4 neonatal mice deficient for *Uhrf1* in hepatocytes (Uhrf1^{HEPKO}) and controls, inset shows band for Cre transgene by RT-PCR. (**G**) Heatmap of Log2 fold change of key cell cycle genes and *Uhrf1* in individual P4 neonatal mice livers ranked by *Uhrf1* expression levels. The number of clutches (zebrafish) or individual animals (mouse) are indicated for each condition and represented as median with range. *P*-value *< 0.05, **< 0.005, *** < 0.0005 by unpaired Student's *t*-test with adjustment for multiple comparisons.

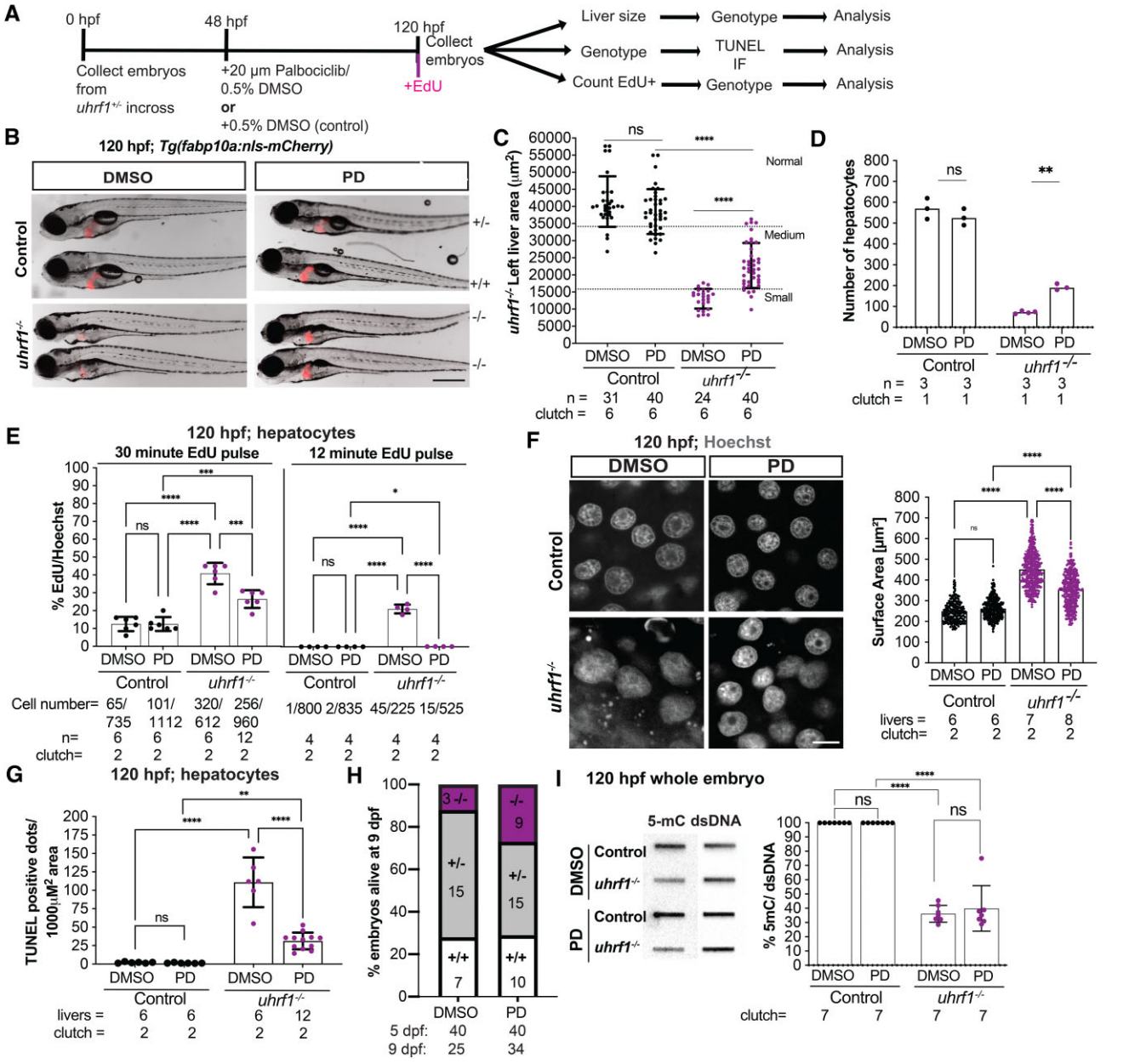

Figure 3. Cdk4/6 inhibition by Palbociclib (PD) rescues the *uhrf1* mutant liver phenotype. (**A**) Treatment scheme for inhibitor Palbociclib (PD). (**B**) Representative images of 120 hpf *uhrf1*$^{-/-}$ and control embryos after DMSO or PD treatment, liver indicated in red. (**C**) Quantification of the left liver lobe area of 120 hpf PD treated and untreated livers, segregated based on the liver size. Normal, medium and small liver size ranges are defined based on mean of DMSO treated controls and mutants ±1 standard deviation, as shown by the error bars. (**D**) Quantification of the number of hepatocytes at 120 hpf *uhrf1*$^{-/-}$ and control embryos after DMSO or PD treatment based on Z-stack images of larvae with the hepatocyte nuclear marker, *Tg(fabp10a:nls-mCherry)*. (**E**) Quantification of 30 min and 12 min EdU incorporation at 120 hpf in DMSO and PD treated controls and *uhrf1*$^{-/-}$. (**F**) Representative confocal image of 120 hpf Hoechst stained control and *uhrf1*$^{-/-}$ hepatocytes from DMSO or PD treatment and quantification of the nuclear surface area. (**G**) TUNEL assay was performed to detect cell death in 120 hpf in DMSO and PD treated controls and *uhrf1*$^{-/-}$ and quantified. (**H**) Genotype of all larvae that survived at 9 dpf following treatment with vehicle or PD from 48–120 hpf. The number of larvae that were treated and the number that remained at 9 dpf are indicated below the graph. (**I**) Representative slot blot for 5-mC and double stranded (ds) DNA in 120 hpf *uhrf1*$^{-/-}$ whole embryos and sibling controls, with quantification of the methylation levels from seven clutches. Scale: 1000 µm in B, 50 µm in F, the number of samples and clutches indicated for each condition and represented as median with range. *P*-value *< 0.05, **< 0.005, *** < 0.0005 by unpaired Student's *t*-test with adjustment for multiple comparisons.

During a short (12 min) EdU pulse, however, Palbociclib treatment completely eliminated any EdU incorporation in *uhrf1* mutants (Figure 3E), suggesting that Cdk4/6 is required for either increased fork speed or multiple origin firing in *uhrf1* mutant hepatocytes. Moreover, the nuclear size, shape, and DNA patterning in *uhrf1* mutant hepatocytes were virtually restored to the WT phenotype by Palbociclib treatment (Figure 3F) and the amount of cell death was significantly reduced by Palbociclib (Figure 3G). Strikingly, Palbociclib also increased survival of *uhrf1* mutants at 9 dpf (Figure 3H). Therefore, Cdk4/6 activity is required for both the developmental and cellular phenotypes caused by Uhrf1 loss.

Since Uhrf1 is a required component of the maintenance methylation machinery (10,11), DNA hypomethylation is a direct consequence of Uhrf1 loss. Assessment of bulk DNA methylation levels confirmed this, as both DMSO and Palbociclib treated *uhrf1* mutants had significant DNA hypomethylation (Figure 3I). Since Palbociclib treatment rescued most of the developmental and cellular defects in *uhrf1* mutants despite persistent DNA hypomethylation, we conclude that the developmental and cellular phenotypes caused by Uhrf1 loss is due to persistent activation of Cdk4/6 and is not a direct consequence of DNA hypomethylation.

Cdk4/6 inhibition blocks cell cycle and Tnfa target genes activation in *uhrf1* mutant livers but does not suppress TE activation or the interferon response

We hypothesized that the cellular and developmental phenotypic rescue of *uhrf1* mutants by Palbociclib was attributed to downregulation of the G1/S transition and S-phase promoting genes. In contrast, we expected that activation of transposable elements (TEs) and the ensuing interferon response (45,49) would not be affected by Palbociclib, since these are directly mediated by DNA methylation loss in *uhrf1* mutants.

We assessed this using bulk RNAseq analysis of the livers of 120 hpf *uhrf1* mutants and their phenotypically normal siblings (control) treated with DMSO or Palbociclib. Principal component analysis showed that controls cluster together regardless of treatment, while mutants treated with Palbociclib were closer to control samples (Figure 4A). Palbociclib treatment of control larvae resulted in modest downregulation of genes that play roles in hepatocyte function and metabolism, but had no effect on genes that regulate the cell cycle (Supplementary Figure S3A, B; Supplementary Tables S5, S6). In contrast, Palbociclib dramatically changed the hepatic transcriptome in *uhrf1* mutants, reducing the number of DEGs from 2272 in DMSO treated mutants to 650 in the liver of *uhrf1* mutants treated with Palbociclib, 560 DEGs common to both (Figure 4B, Supplementary Table S7). While the common DEGs showed a very high correlation in their expression ($r = 0.974$), the genes that were unique to each dataset genes were less correlated ($r = 0.666$; Supplementary Figure S3C). In contrast, the upregulation of transposable elements (TEs) in *uhrf1* mutant livers was not suppressed by Palbociclib (Supplementary Figure S3D-E).

We predicted that Cdk4/6 inhibition in *uhrf1* mutants would reduce the induction of E2F targets, but would have no effect on the interferon response as this is caused by TE activation. Unsupervised clustering of the unified set of DEGs from both DMSO and Palbociclib treated mutants showed that most of the upregulated genes in DMSO treated *uhrf1* mutant livers were still upregulated, but to a lesser extent in Palbociclib treated mutants (Figure 4C, cluster 5), however, a subset of genes remains elevated in both samples (cluster 4 and 5) (Figure 4C, Supplementary Table S8). GO analysis of these two clusters shows that DNA replication related genesets were predominant in cluster 5, and that immune pathways were predominant in cluster 4 (Figure 4D-E, Supplementary Table S9). Specific analysis of key genes involved in the pre-replication phase of cell cycle, such as *ccna2*, the *orcs*, *mcms* and *cdc45* which is important for origin firing at the replication forks in association with *mcms* (69,70), showed that they were highly induced in DMSO treated mutants, but expressed at significantly lower levels in the liver of *uhrf1* mutants treated with Palbociclib (Figure 4F, Supplementary Figure S3F and Supplementary Table S10).

Interestingly, the immune genes which were all upregulated in *uhrf1* mutants showed a nuanced response to Palbociclib treatment: interferon response genes remained highly expressed while genes downstream of Tnfa were downregulated in the liver of *uhrf1* mutants exposed to Palbociclib (Figure 4F, Supplementary Table S11). Since CDK6 positively regulates TNFa (71), we conclude that Tnfa induction in *uhrf1* mutants is attributed to Cdk4/6 activation, in contrast to interferon related genes which are due to TE activation.

We further investigated the effect of Palbociclib on the expression of cell cycle regulatory genes in *uhrf1* mutants using IPA. We first analyzed the genes activated in *uhrf1* mutants compared to controls treated with DMSO and found significant activation of genes regulating G1/S *ccnd1*, *ccne* and *cdk4/6*, which lead to upregulation of transcription factors *e2fs, hdac, ftdp1*, as well as activation of DNA damage sensors *atm, atr* and *tp53* (Supplementary Figure S4A). qPCR analysis of several of these genes confirmed that Palbociclib downregulated their expression the liver of *uhrf1* mutants (Supplementary Figure S4B). We next compared the gene expression patterns in *uhrf1* mutants treated with Palbociclib to mutants treated with DMSO, and identified 280 DEGs (Supplementary Figure S4C; Supplementary Table S12). IPA analysis of these DEGs showed that genes involved in cell cycle checkpoints were upregulated and genes involved in cell cycle control and S-phase were downregulated in *uhrf1* mutant livers treated with Palbociclib (Figure 4G) and while Palbociclib suppressed Atr signaling, it had no effect on *atm* and *tp53* induction in *uhrf1* mutants (Figure 4G, Supplementary Figure S4D, Supplementary Table S13), suggesting that some DNA damage persists even when DNA replication is suppressed.

Together, these data indicate that Cdk4/6 activation does not affect DNA methylation, TE induction, interferon response and DNA damage caused by Uhrf1 loss, but is required for the downregulation of G1/S checkpoints, E2F targets, increased DNA replication and cell death. Based on our previous finding that blocking Tnfa reduced cell death in *uhrf1* mutant livers but has no effect on the mutant phenotype or liver size at 120 hpf (45), combined with the current finding that Palbociclib reduced Tnfa activation, we deduce Palbociclib prevents cell death in *uhrf1* mutants by inactivation of Tnfa.

Cdk4/6 is activated by *dnmt1* mutation

To understand if the cellular phenotypes that cause hepatic outgrowth failure in *uhrf1* mutants are attributed to DNA hypomethylation, we assessed larvae with a loss of function mutation in *dnmt1* (27). These have a strikingly similar phenotype to *uhrf1* mutants, including DNA

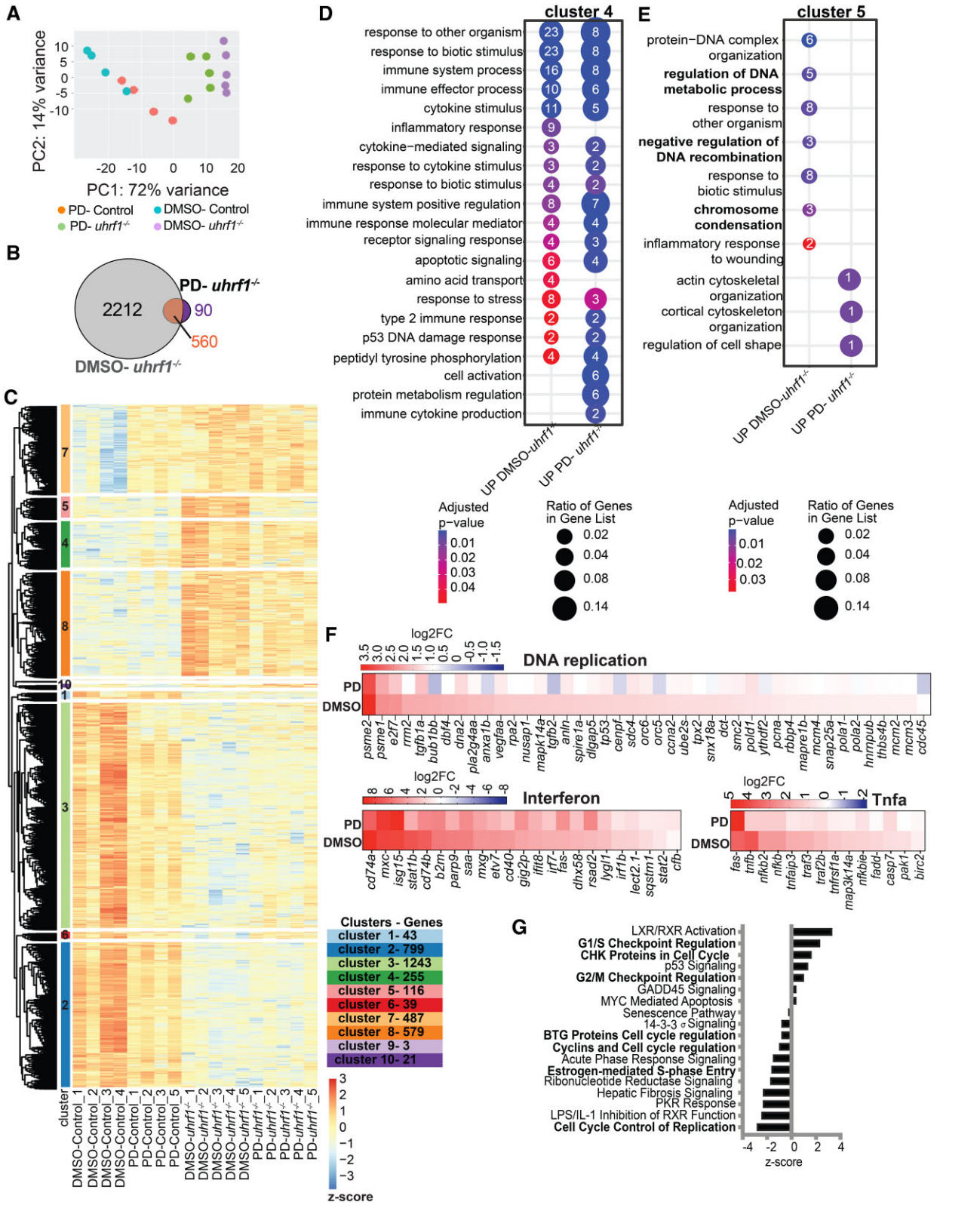

Figure 4. Cdk4/6 inhibition by Palbociclib (PD) rescues abnormal cell cycle gene expression in *uhrf1* mutants. (**A**) PCA analysis of RNA Seq from 120 hpf Palbociclib (PD) treated and DMSO treated *uhrf1*$^{-/-}$ and control livers. (**B**) Venn diagram of differential expressed genes (DEGs) (cutoff *P*-adj < 0.05) between *uhrf1*$^{-/-}$ and their control siblings treated with DMSO and PD. (**C**) Unsupervised clustering heatmap of the expression profile of 120 hpf DMSO and PD treated *uhrf1*$^{-/-}$ liver. z-scores based on raw counts. Rows are divided into 10 clusters calculated on the hierarchical clustering of dendrogram (Euclidean distance). (**D**) REVIGO gene ontology of cluster 4 and (**E**) and cluster 5. (**F**) Key cell cycle genes, immune and *tnfa* response gene expression between PD and DMSO treated *uhrf1*$^{-/-}$ plotted as a heatmap with $\log_2$fold change. (**G**) IPA of the cell cycle genes differentially expressed between 120 hpf *uhrf1*$^{-/-}$ PD and DMSO livers, cell cycle checkpoint regulation pathways indicated in bold. *P*-value *< 0.05, **< 0.005, *** < 0.0005 by unpaired Student's *t*-test with adjustment for multiple comparisons and represented as median with range.

hypomethylation, large and disorganized hepatocyte nuclei and a small liver (28,29,44,45,72). We asked whether the cell cycle related geneset that was differentially expressed in *uhrf1* mutant livers (i.e. the unified set of all cell cycle genes in Figure 2B) were also differentially expressed in bulk RNAseq data from the liver of 120 hpf *dnmt1* mutants (45). Many of the genes required for DNA replication (*pcna, orcs, mcms*, *cdc45* and *pold2*) were upregulated in *dnmt1* mutant livers (Figure 5A). In contrast to the high number of hepatocytes undergoing DNA replication in *uhrf1* mutants, *dnmt1* mutant livers had significantly lower number of hepatocytes that incorporate EdU at both 96 hpf and 120 hpf (Figure 5B). Thus, Dnmt1 loss prevented DNA replication, consistent with a requirement for Dnmt1 at the replication fork (13,14). Previous analysis showed that *uhrf1* and *dnmt1* mutant livers have a similar gene expression profile characterized by upregulation of genes required for DNA replication (28,45). IPA provided a more detailed comparison of this pattern, showing that while the Atm and Tp53 mediated DNA damage responses were upregulated in both samples, some genes that regulate S-phase (*chek1, chek2, tlk1/2, cdc25*), M phase progression (*cdk1, cyclin B*) and Atr mediated DNA damage response signaling were upregulated only in *uhrf1* mutant livers (Figures 5A and S5). Thus, while both mutants have a global upregulation of cell cycle promoting genes and the Atm mediated response to double stranded breaks, *uhrf1* loss specifically induces a response to single stranded breaks.

If Cdk4/6 is upstream of cell cycle activation in *uhrf1* and *dnmt1* mutants, treatment of *dnmt1* mutants with Palbociclib should downregulate these genes. Palbociclib had no significant effect on the developmental phenotype or liver size in *dnmt1* mutants (Figure 5C-D). While there was variability in the induction of cell cycle genes in *dnmt1* mutant livers, treatment with Palbociclib decreased the expression of assessed cell cycle genes, with *ccne1, cdc6* and *pold1* reaching significance. As in *uhrf1* mutants, Palbociclib had no effect on interferon response gene expression in *dnmt1* mutant livers (Figure 5E). Thus, while *dnmt1* and *uhrf1* loss activate Cdk4/6 and E2F target genes, derepress TEs and induce an interferon response, these responses are independent. Induction of cell cycle genes requires Cdk4/6 signaling while TE activation and the interferon response do not. Moreover, the finding that *dnmt1* mutants are not rescued by Palbociclib reflects the fact that Dnmt1 deficient cells cannot undergo DNA replication, likely due to the requirement of Dnmt1 at the replication fork (14,73,74).

To investigate the mechanism of Cdk4/6 activation in *dnmt1* and *uhrf1* mutants, we assessed the expression of Cdkn2a/b in hepatocytes. Immunofluorescence shows a significant depletion of Cdkn2a/b protein in the liver of both mutants at 120 hpf (Figure 5F, G), suggesting the loss of this inhibitor as a mechanism by which Cdk4/6 is upregulated in these mutants.

DNA replication in *uhrf1* mutant hepatocytes requires *dnmt1*

To determine if Dnmt1 was required for the EdU incorporation phenotype in *uhrf1* mutant hepatocytes, we used CRISPR-Cas9 to target *dnmt1*. Efficacy was verified using an *in vivo* reporter of DNA methylation in which the UAS:GFP cassette is silenced by DNA methylation, and GFP expression occurs in response to Gal4 when methylation is lost on the UAS promoter (*Tg(c269off$^{+/-}$; 14X UAS:dsRed)* (45,75). All *Tg(c269off$^{+/-}$; 14X UAS:dsRed$^{+/-}$);dnmt1^{cr}* larvae had GFP expression in the head at 120 hpf (Supplementary Figure S6A), but had a mild phenotype compared to *dnmt1* mutants (Figure 5C). Crispr deletion of *dnmt1* did not change liver size of *uhrf1* mutants (Figure 6A, B) or the volume or shape of the *uhrf1* mutant hepatocyte nuclei (Supplementary Figure S6B–D). *dnmt1* deletion did not rescue aberrant expression of cell cycle genes in *uhrf1* mutant livers (Figure 6C) but did significantly reduce EdU incorporation in hepatocytes compared to uninjected *uhrf1−/−*(Figure 6D). We conclude that Dnmt1 is required for DNA replication in *uhrf1* mutant hepatocytes, consistent with a role for Dnmt1 at the replication fork.

Replication stress as a mechanism for Atr activation and hepatic outgrowth failure in *uhrf1* mutants

ATR responds to DNA replication stress by stabilizing replication forks, delaying or blocking the progress of the cell cycle, promoting DNA repair (76,77). In response to replication stress, ATR activates dormant origins within active replication clusters while repressing firing within those that are not yet activated (78). Since Atr was specifically activated in *uhrf1* mutants, but not *dnmt1* mutants (Figures 5A and S5), we hypothesized that the DNA replication phenotype in *uhrf1* mutants, which is absent from *dnmt1* mutants, causes replication stress, DNA damage and Atr activation. To test this, we assessed the staining pattern and expression levels of γH2AX as a marker of DNA damage, phosphorylated replication protein A (pRPA) as a marked of replication stress and phosphorylated Chk1, as an assay for Atr activation in *uhrf1* mutants (Figure 7A–C). All were induced, and, importantly, γH2AX staining was found to co-localize with EdU incorporation in *uhrf1* mutant hepatocytes at 120 hpf, but did not co-localize with EdU in controls or in cells with DNA damage induced by H_2O_2 and was not present at 96 hpf (Figure 7A). Together, these data indicate that in *uhrf1* mutant hepatocytes, DNA damage accumulates at the site of DNA replication and that there is replication stress and Atr.

These data predict that Atr is activated in response to replication stress in Uhrf1 deficient hepatocytes. We hypothesized that Atr could be responsible for the increased EdU incorporation following replication fork collapse by triggering replication from dormant origins. To test this, we established a treatment protocol using the highly selective and potent ATR inhibitor VE- 821 (79) which we demonstrated effectively blocked Chk1p activation in response to H_2O_2 induced DNA damage in control embryos (Supplementary Figure S7A). While treatment from 48 to 120 hpf with 10 μm VE-821 had no obvious effects on control larvae and had minimal effects on the overall *uhrf1* mutant phenotype, it significantly increased liver size (Figure 7D, E), reduced EdU incorporation in *uhrf1* mutant hepatocytes from 36% to 24%, respectively (Figure 7C, D) and modestly restored nuclear morphology (Supplementary Figure S7B). This demonstrates that DNA replication in *uhrf1* mutants is, in part, dependent on Atr.

Discussion

We report that Cdk4/6 activation is the mechanism accounting for the unusual cell cycle defect caused by *uhrf1* mutation in zebrafish and present a model that illustrates the relationship between DNA methylation, cell cycle regulation, DNA

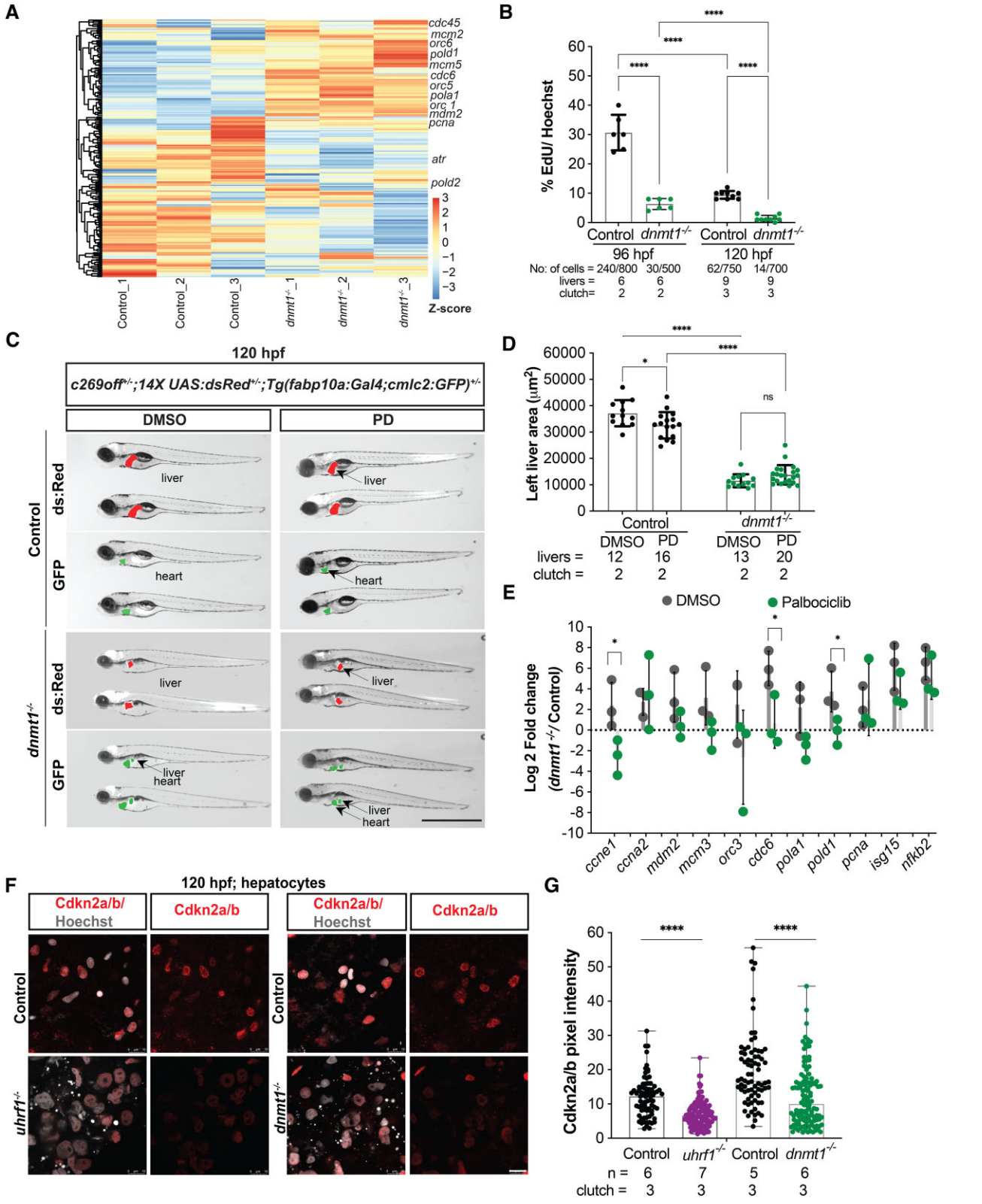

Figure 5. Cdkna2a/b depletion as a mechanism of Cdk4/6 activation in *dnmt1* and *uhrf1* mutants. (**A**) Unsupervised clustering heatmap of all the cell cycle genes of 120 hpf *dnmt1*$^{-/-}$ liver with z-scores based on rows, important S-phase genes are indicated. (**B**) EdU quantification (pulse 30 minute) of 96 hpf and 120 hpf control and *dnmt1*$^{-/-}$ hepatocytes. (**C**) Representative images of 120 hpf *dnmt1*$^{-/-}$ and controls with *c269off*$^{+/-}$*; 14X UAS:dsRed*$^{+/-}$*; Tg(fabp10a:Gal4;cmlc2:GFP)*$^{+/-}$ treated with DMSO or Palbociclib (PD), showing the liver (dsRed), the heart (GFP) as a marker of transgenesis and in green, the liver with hypomethylation in mutants only. (**D**) Quantification of the left liver lobe area of *dnmt1*$^{-/-}$ and controls, treated with PD or DMSO. Scale: 50 μm, the number of samples and clutches indicated for each condition. (**E**) QPCR of key cell cycle genes and immune genes in 120 hpf *dnmt1*$^{-/-}$ livers. (**F**) Representative immunofluorescent images of Cdkn2a/b in 120 hpf *uhrf1*$^{-/-}$, *dnmt1*$^{-/-}$ and their respective control livers and (**G**) quantification of the Cdkn2a/b pixel intensity in hepatocytes. Scale: 1000 μm in C, 100 μm in F, the number of samples and clutches indicated for each condition. *P*-value *< 0.05, **< 0.005, *** < 0.0005 by unpaired Student's *t*-test with adjustment for multiple comparisons and represented as median with range.

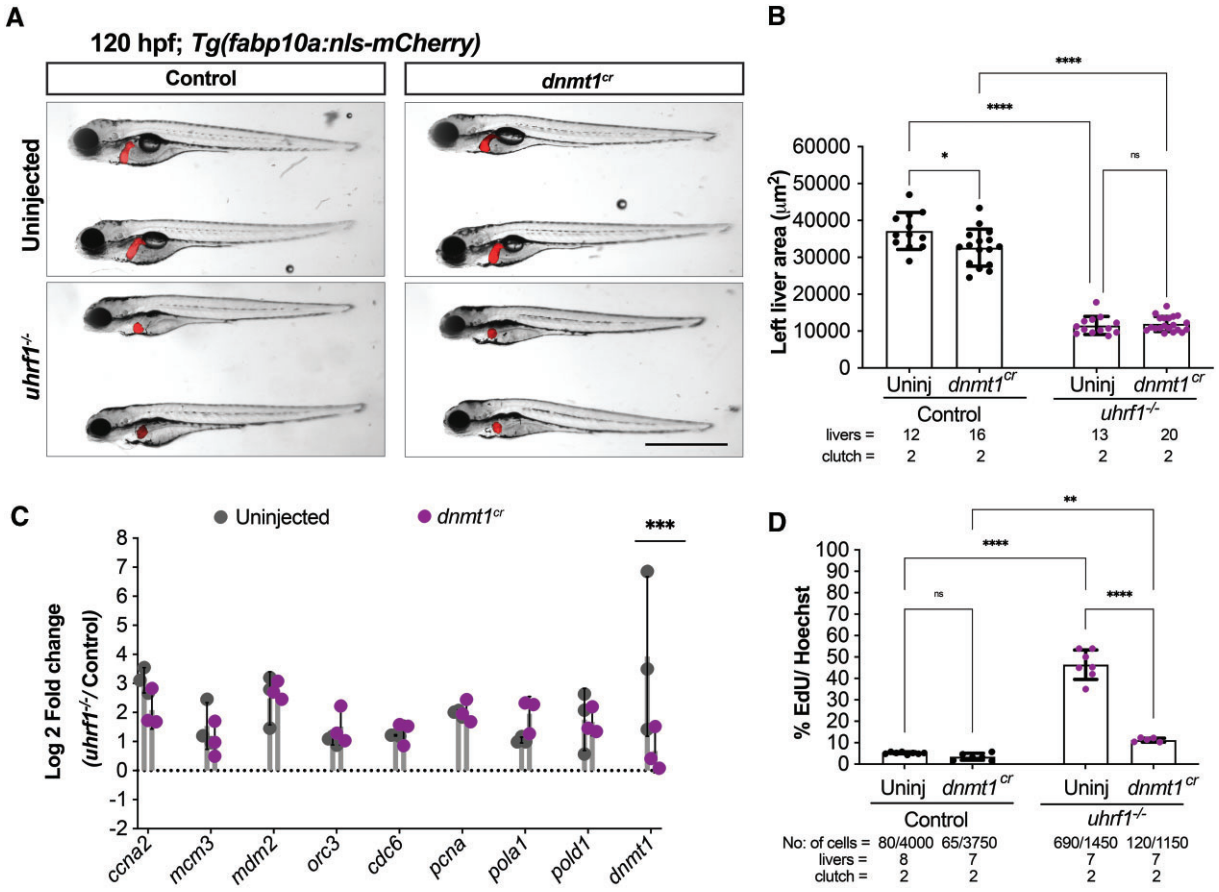

Figure 6. *dnmt1* depletion rescues DNA replication defects in *uhrf1* mutant hepatocytes. (**A**) Representative images of 120 hpf *uhrf1*$^{-/-}$ and control embryos uninjected or injected with *dnmt1*^{cr}. (**B**) Quantification of the left liver lobe area of 120 hpf *uhrf1*$^{-/-}$ and controls uninjected or injected with *dnmt1*^{cr}. (**C**) qPCR of key cell cycle genes in 120 hpf livers of *uhrf1*$^{-/-}$ and controls uninjected or injected with *dnmt1*^{cr}. (**D**) 30 minute EdU incorporation at 120 hpf in uninjected and *dnmt1*^{cr} injected controls and *uhrf1*$^{-/-}$ livers. Scale: 50 μm in B, 1000 μm in C, the number of samples and clutches indicated for each condition *P*-value *< 0.05, **< 0.005, *** < 0.0005 by unpaired Student's *t*-test with adjustment for multiple comparisons and represented as median with range.

replication and development (Figure 7G). Our data are consistent with a model in which the absence of Uhrf1 or Dnmt1 in hepatocytes leads to Cdkn2a/b downregulation and constitutive Cdk4/6 activation to drive cells into S-phase. DNA replication cannot proceed without Dnmt1, so in *dnmt1* mutants, hepatocytes arrest without replicating their DNA. In contrast, *uhrf1* mutants have sufficient Dnmt1 (28) so that DNA replication can be initiated, but is futile, causing replication stress, DNA damage and Atr activation. We propose that Atr activation has two consequences: (i) firing of dormant origins, which then repeats the cycle of replication fork collapse, DNA damage and further Atr activation and (ii) cell cycle checkpoint activation, preventing cells from exiting S-phase. Moreover, The data presented here, combined with our finding that reducing cell death does not rescue liver size (45), indicates that the cell cycle defect is the main mechanism of hepatic outgrowth failure.

The striking rescue of the cellular and developmental defects in Uhrf1 deficient zebrafish embryos by Cdk4/6 inhibition suggests that a persistent signal to enter S-phase causes all the downstream phenotypes. The data showing that mice with Uhrf1 deficient in hepatocytes have a similar cell cycle gene expression profile to *uhrf1* mutant zebrafish suggests that this role is conserved. Surprisingly, the cellular and developmental phenotypes resolve, despite persistent DNA hypomethylation, TE activation and an interferon response. This finding differentiates between the direct targets of Uhrf1—i.e. DNA hypomethylation – and those that are secondary consequences—i.e. Cdk4/6 activation and DNA replication. These data also show that loss of DNA methylation and TE activation *per se* do not cause the developmental defects that occur in *uhrf1* mutants. Rather it is the downstream consequences of DNA hypomethylation which are responsible.

The finding of similar Cdk4/6 dependent gene expression and downregulation of Cdkn2a/b protein in *dnmt1* and *uhrf1* mutants suggests that DNA hypomethylation is the mechanism for Cdkn2a/b downregulation and Cdk4/6 activation. In mammalian cells, *Cdkn2a* transcription is suppressed by repressive epigenetic marks, including DNA methylation (80,81). While it would be surprising if *uhrf1* and *dnmt1* mutation caused hypermethylation of the *cdkn2a/b* regulatory sequences, it is possible that loss of methylation causes redistribution of another repressive epigenetic marks to the p16^{INK4a} regulatory regions, as we described in other contexts (48). However, RNAseq data does not show a significant downregulation of *cdkn2a/b* expression in *uhrf1* mutant livers, suggesting a post-transcriptional regulation of Cdkn2a/b in these mutants. Further investigation is required to determine the relationship between Uhrf1, Dnmt1, DNA hypomethylation and Cdkn2a/b regulation.

We previously published that *uhrf1* mutant hepatocytes have both an abnormal DNA replication pattern and

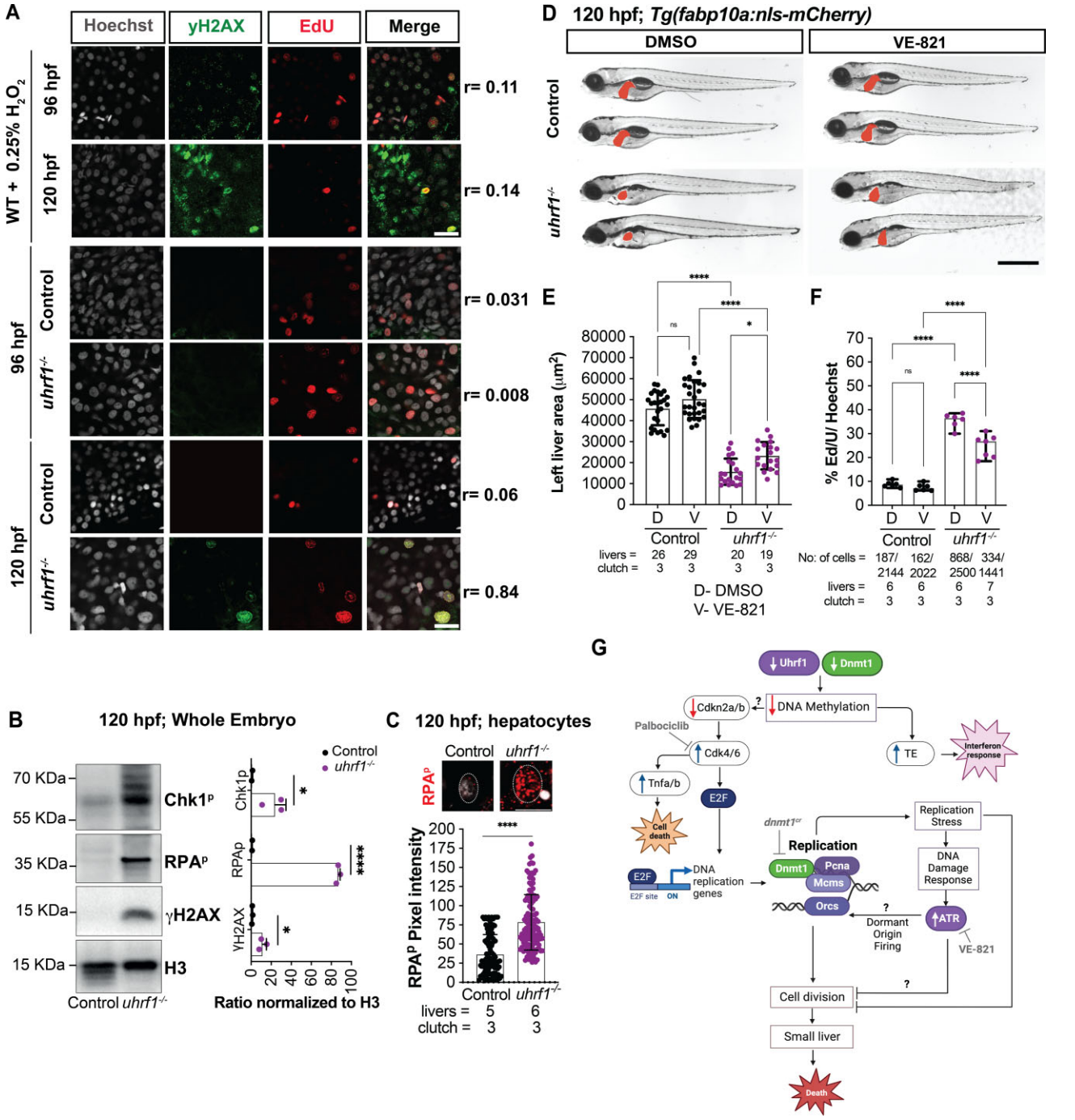

Figure 7. Atr inhibition increases liver size and decreases DNA replication in *uhrf1* mutant hepatocytes. (**A**) Representative images of γH2AX immunofluorescence and EdU labeling at 96 hpf and 120 hpf embryos following H_2O_2 treatment as a positive control and of *uhrf1*$^{-/-}$ mutants and sibling control livers. r-values indicate Pearson's correlation of co-localized pixels from γH2AX and EdU fluorescence. (**B**) Western blot of whole embryo extracts from 120 hpf *uhrf1*$^{-/-}$ and control siblings for Chk1^{P}, RPA^{P}, γH2AX and H3 as a loading control. (**C**) Quantification of the RPA^{P} pixel intensity in 120 hpf *uhrf1*$^{-/-}$ and their respective control hepatocytes. Insets show representative images of RPA^{P} stained hepatocytes. (**D**) Representative images of 120 hpf *uhrf1*$^{-/-}$ and control larvae with *Tg(fabp10a:nls-mCherry)* after DMSO or VE- 821 treatment, liver highlighted in red. (**E**) Quantification of the left liver lobe area of 120 hpf VE- 821 treated and untreated embryos from *uhrf1*$^{-/-}$ and control larvae. (**F**) Quantification of EdU positive cells following 30 min of incorporation at 120 hpf in DMSO and VE- 821 treated control and *uhrf1*$^{-/-}$ livers. Scale: 50 μm in A, 100 μm in C, 1000 μm in D, the number of samples and clutches indicated for each condition. *P*-value *< 0.05, **< 0.005, *** < 0.0005 by unpaired Student's *t*-test with adjustment for multiple comparisons. Data represented as median with range. (**G**) Model of the relationship between *uhrf1* mutation, DNA methylation, cell cycle regulation, DNA replication and hepatic outgrowth failure. Uhrf1 and Dnmt1 loss causes DNA hypomethylation, upregulation of TEs and inflammatory response. This also inhibits Cdkn2a/b at protein levels, causing Cdk4/6 activation, induction of DNA replication, replication stress, DNA damage and Atr mediated dormant origin firing. In a parallel pathway, Cdk4/6 also activates Tnfa and cell death. We speculate that the DNA damage response inhibits cell division, restricting organ outgrowth and causing lethality in *uhrf1* mutants.

widespread cell death (26,28). We demonstrate that both *uhrf1* and *dnmt1* mutants activate cell cycle genes in a Cdk4/6 dependent manner, but while *uhrf1* mutant hepatocytes undergo increased DNA replication, *dnmt1* mutant hepatocytes do not. Since DNA replication in *uhrf1* mutant hepatocytes was rescued by *dnmt1* depletion, we conclude that the *uhrf1* mutant phenotype could be attributed to elevated Dnmt1 levels (28,82,83) or, more likely, due to the requirement for Dnmt1 in forming a functional replication fork (73,74). Hence, Dnmt1 is both upstream and downstream of Cdk4/6 in this model. Taken together, these results provide mechanistic insight into cell cycle regulation during development and uncover a more epigenetic regulation and cell cycle control.

Uhrf1 loss has been implicated in the mis-regulation of both G1 and G2/M phases of the cell cycle (21,31,84) and here we provide evidence for a functional role in regulating DNA replication. There are several possible mechanisms underlying this phenotype. The first, discussed above, is that DNA replication stress activates Atr to prevent cell cycle progression while promoting dormant origin firing and triggering further replication stress as the forks at dormant origins should be dysfunctional in the absence of Uhrf1 (Figure 7G). During normal DNA replication, fork speed has to be moderated for the fidelity of normal cell cycle, with an increased fork speed triggering replication stress and DNA damage response (85,86). However during DNA rereplication, DNA synthesis was reported to progress slowly, and repeatedly utilize the same main origins (87). In contrast, unscheduled firing of dormant origins can lead to increased and uncoordinated DNA synthesis (4,88). While experimental approaches required to assess fork speed and origin utilization is challenging in whole embryos, the Atr inhibition data in *uhrf1* mutants supports the hypothesis that the increased DNA replication in *uhrf1* deficient hepatocytes is caused by Atr dependent firing of dormant origins, not a repeated firing of the same origins. The question of why origins of replication can be fired at all if there is a checkpoint activated by Atr is addressed by data from a study where Atr/Chk1 pathway activation in response to replication stress caused dormant origin firing within active replication clusters (89–91). We hyopothesize that dormant origin firing is a mechanism to assure that DNA replication is sufficient to allow liver expansion during this critical stage of development when organ expansion is essential for embryo survival. This mechanism may be different in mature cells or in cancer, where Uhrf1 deficiency has been shown to block Cdk4 activation and DNA replication (92).Moreover, in cancer, overexpression of UHRF1 may act as a dominant negative, blocking DNA methylation and altering histone modifications, with the result, the cells become progenitor like (93,94).

An alternative, intriguing mechanism that could contribute to the DNA replication defect in *uhrf1* mutants involves a defect in regulating which origins fire due to a failure to degrade replication licensing factor Cdt1, which is required to prevent reuse of replication origins. Since the levels of Cdt1 protein are regulated by the Cul4–Ddb1–Cdt2 E3 ubiquitin ligase complex (95), it is feasible that Cdt1 stabilization due to nuclear Cyclin D1/CDK4, as shown in other models (96), could result in repeated origin use. Further, Cyclin D1/CDK4 activation during S-phase specifically represses transcription of *CUL4*, resulting in CDT1 stabilization (97). Our finding that *uhrf1* loss induced overexpression of *ccnd1* and *cdk4* and downregulation of *cul4* suggests that Ctd1 levels may persist and promote DNA rereplication (98). Combining the lack of this 'off signal' for DNA replication with Atr mediated dormant origin firing and constitutive Cdk4/6 activation could induce the unscheduled and unproductive DNA replication that is observed in *uhrf1* deficient cells.

We were intrigued by the finding that Palbociclib blocked cell death in *uhrf1* mutant hepatocytes. In other studies, Palbociclib has been shown to activate NF-κB and TNF-induced gene expression in mammalian cells (99). Given our previous finding that Tnfa depletion in *uhrf1* mutants prevented hepatocyte cell death but did not rescue liver size(45), we attribute the rescue of cell death in Palbociclib treated *uhrf1* mutants to the downregulation of Tnfa signaling, and conclude that cell death is not caused by cell cycle defects. These data also show that the small liver phenotype in this context is not caused by cell death, but rather is due to failure of hepatocyte proliferation.

In summary, this work provides the first insight into two distinct functions of Uhrf1 during liver development. Here we show that Uhrf1 loss induces Cdk4/6, E2f and all the genes that are required for S-phase. This is paradoxical, as UHRF1 is overexpressed in nearly all types of solid tumors (100), including HCC (51,101), Palbociclib effectively suppressed cell proliferation in tumor growth in preclinical models of HCC by promoting a reversible cell cycle arrest (53). Therefore, it is possible that in HCC, UHRF1 overexpression can act as a dominant negative to activate CDK4/6 and promote cell proliferation, and future studies may investigate whether Palbociclib functions as a therapeutic by counteracting the oncogenic effects of UHRF1.

Data availability

All the datasets used in this paper are available as GEO datasets under the numbers GSE160728 and GSE234993. Code used in this manuscript is available on DOI: 10.5281/zenodo.10459748.

Supplementary data

Supplementary Data are available at NAR Online.

Acknowledgements

The NYUAD Core Technology Platforms was essential to perform the RNA sequencing. We would like to thank Nizar Drou and Muhammad Arshad for assistance with deep sequencing and TE analysis, Marc Arnoux and Mehar Sultana for assistance with technical support for library preparation, Rachid Rezgui for assistance with the use of Confocal Microscopy. We are grateful to Tina Kim and Nouf Khan for technical support with the EdU staging and nuclei count respectively. All members of the Sadler group provided insightful discussion and help throughout the project, in particular Patrice Delaney for bioinformatics and editing assistance and James Griffin for proofreading.

Author contributions: Conceptualization, K.C.S., B.M.; methodology, B.M., E.M., S.R.; formal analysis, B.M., E.M., S.R.; investigation, K.C.S., B.M., E.M., S.R.; writing—original draft preparation, K.C.S. and B.M., writing—review and editing, K.C.S., B.M., E.M.; visualization, K.C.S., B.M., E.M.; supervision, K.C.S.; project administration, K.C.S.; funding acquisition, K.C.S. All authors have read and agreed to the published version of the manuscript.

Funding

National Institutes of Health (NIH) [2R01DK080789-10A1 to K.C.S.]; NYUAD Faculty Research Fund [AD188]; NYUAD Research Institute Award to the Center for Genomics and Systems Biology (ADHPG-CGSB). Funding for open access charge: NYUAD [RE188].

Conflicts of interest statement

None declared.

References

1. Petryk,N., Kahli,M., d'Aubenton-Carafa,Y., Jaszczyszyn,Y., Shen,Y., Silvain,M., Thermes,C., Chen,C.L. and Hyrien,O. (2016) Replication landscape of the human genome. *Nat. Commun.*, **7**, 10208.
2. Guilbaud,G., Murat,P., Wilkes,H.S., Lerner,L.K., Sale,J.E. and Krude,T. (2022) Determination of human DNA replication origin position and efficiency reveals principles of initiation zone organisation. *Nucleic Acids Res.*, **50**, 7436–7450.
3. Recolin,B., van der Laan,S., Tsanov,N. and Maiorano,D. (2014) Molecular mechanisms of DNA replication checkpoint activation. *Genes (Basel)*, **5**, 147–175.
4. McIntosh,D. and Blow,J.J. (2012) Dormant origins, the licensing checkpoint, and the response to replicative stresses. *Cold Spring Harb. Perspect. Biol.*, **4**, a012955.
5. Greenberg,M.V.C. and Bourc'his,D. (2019) The diverse roles of DNA methylation in mammalian development and disease. *Nat. Rev. Mol. Cell Biol.*, **20**, 590–607.
6. Arita,K., Ariyoshi,M., Tochio,H., Nakamura,Y. and Shirakawa,M. (2008) Recognition of hemi-methylated DNA by the SRA protein UHRF1 by a base-flipping mechanism. *Nature*, **455**, 818–821.
7. Avvakumov,G.V., Walker,J.R., Xue,S., Li,Y., Duan,S., Bronner,C., Arrowsmith,C.H. and Dhe-Paganon,S. (2008) Structural basis for recognition of hemi-methylated DNA by the SRA domain of human UHRF1. *Nature*, **455**, 822–825.
8. Hashimoto,H., Horton,J.R., Zhang,X., Bostick,M., Jacobsen,S.E. and Cheng,X. (2008) The SRA domain of UHRF1 flips 5-methylcytosine out of the DNA helix. *Nature*, **455**, 826–829.
9. Qian,C., Li,S., Jakoncic,J., Zeng,L., Walsh,M.J. and Zhou,M.M. (2008) Structure and hemimethylated CpG binding of the SRA domain from human UHRF1. *J. Biol. Chem.*, **283**, 34490–34494.
10. Bostick,M., Kim,J.K., Esteve,P.O., Clark,A., Pradhan,S. and Jacobsen,S.E. (2007) UHRF1 plays a role in maintaining DNA methylation in mammalian cells. *Science*, **317**, 1760–1764.
11. Sharif,J., Muto,M., Takebayashi,S., Suetake,I., Iwamatsu,A., Endo,T.A., Shinga,J., Mizutani-Koseki,Y., Toyoda,T., Okamura,K., *et al.* (2007) The SRA protein Np95 mediates epigenetic inheritance by recruiting Dnmt1 to methylated DNA. *Nature*, **450**, 908–912.
12. Mancini,M., Magnani,E., Macchi,F. and Bonapace,I.M. (2021) The multi-functionality of UHRF1: epigenome maintenance and preservation of genome integrity. *Nucleic Acids Res.*, **49**, 6053–6068.
13. Lopez-Contreras,A.J., Ruppen,I., Nieto-Soler,M., Murga,M., Rodriguez-Acebes,S., Remeseiro,S., Rodrigo-Perez,S., Rojas,A.M., Mendez,J., Muñoz,J., *et al.* (2013) A proteomic characterization of factors enriched at nascent DNA molecules. *Cell Rep.*, **3**, 1105–1116.
14. Sirbu,B.M., McDonald,W.H., Dungrawala,H., Badu-Nkansah,A., Kavanaugh,G.M., Chen,Y., Tabb,D.L. and Cortez,D. (2013) Identification of proteins at active, stalled, and collapsed replication forks using isolation of proteins on nascent DNA (iPOND) coupled with mass spectrometry. *J. Biol. Chem.*, **288**, 31458–31467.
15. Ferry,L., Fournier,A., Tsusaka,T., Adelmant,G., Shimazu,T., Matano,S., Kirsh,O., Amouroux,R., Dohmae,N., Suzuki,T., *et al.* (2017) Methylation of DNA ligase 1 by G9a/GLP recruits UHRF1 to replicating DNA and regulates DNA methylation. *Mol. Cell*, **67**, 550–565.
16. Kim,J.K., Esteve,P.O., Jacobsen,S.E. and Pradhan,S. (2009) UHRF1 binds G9a and participates in p21 transcriptional regulation in mammalian cells. *Nucleic Acids Res.*, **37**, 493–505.
17. Nishiyama,A., Yamaguchi,L., Sharif,J., Johmura,Y., Kawamura,T., Nakanishi,K., Shimamura,S., Arita,K., Kodama,T., Ishikawa,F., *et al.* (2013) Uhrf1-dependent H3K23 ubiquitylation couples maintenance DNA methylation and replication. *Nature*, **502**, 249–253.
18. Taylor,E.M., Bonsu,N.M., Price,R.J. and Lindsay,H.D. (2013) Depletion of Uhrf1 inhibits chromosomal DNA replication in Xenopus egg extracts. *Nucleic Acids Res.*, **41**, 7725–7737.
19. Magri,L., Swiss,V.A., Jablonska,B., Lei,L., Pedre,X., Walsh,M., Zhang,W., Gallo,V., Canoll,P. and Casaccia,P. (2014) E2F1 coregulates cell cycle genes and chromatin components during the transition of oligodendrocyte progenitors from proliferation to differentiation. *J. Neurosci.*, **34**, 1481–1493.
20. Unoki,M., Nishidate,T. and Nakamura,Y. (2004) ICBP90, an E2F-1 target, recruits HDAC1 and binds to methyl-CpG through its SRA domain. *Oncogene*, **23**, 7601–7610.
21. Bonapace,I.M., Latella,L., Papait,R., Nicassio,F., Sacco,A., Muto,M., Crescenzi,M. and Di Fiore,P.P. (2002) Np95 is regulated by E1A during mitotic reactivation of terminally differentiated cells and is essential for S phase entry. *J. Cell Biol.*, **157**, 909–914.
22. McCabe,M.T., Davis,J.N. and Day,M.L. (2005) Regulation of DNA methyltransferase 1 by the pRb/E2F1 pathway. *Cancer Res.*, **65**, 3624–3632.
23. Kimura,H., Nakamura,T., Ogawa,T., Tanaka,S. and Shiota,K. (2003) Transcription of mouse DNA methyltransferase 1 (Dnmt1) is regulated by both E2F-Rb-HDAC-dependent and -independent pathways. *Nucleic Acids Res.*, **31**, 3101–3113.
24. Ge,T.T., Yang,M., Chen,Z., Lou,G. and Gu,T. (2016) UHRF1 gene silencing inhibits cell proliferation and promotes cell apoptosis in human cervical squamous cell carcinoma CaSki cells. *J. Ovarian Res.*, **9**, 42.
25. Zhang,J., Yang,C., Wu,C., Cui,W. and Wang,L. (2020) DNA methyltransferases in cancer: biology, paradox, aberrations, and targeted therapy. *Cancers (Basel)*, **12**, 2123.
26. Sadler,K.C., Krahn,K.N., Gaur,N.A. and Ukomadu,C. (2007) Liver growth in the embryo and during liver regeneration in zebrafish requires the cell cycle regulator, uhrf1. *Proc. Natl. Acad. Sci. U.S.A.*, **104**, 1570–1575.
27. Anderson,R.M., Bosch,J.A., Goll,M.G., Hesselson,D., Dong,P.D., Shin,D., Chi,N.C., Shin,C.H., Schlegel,A., Halpern,M., *et al.* (2009) Loss of Dnmt1 catalytic activity reveals multiple roles for DNA methylation during pancreas development and regeneration. *Dev. Biol.*, **334**, 213–223.
28. Jacob,V., Chernyavskaya,Y., Chen,X., Tan,P.S., Kent,B., Hoshida,Y. and Sadler,K.C. (2015) DNA hypomethylation induces a DNA replication-associated cell cycle arrest to block hepatic outgrowth in uhrf1 mutant zebrafish embryos. *Development*, **142**, 510–521.
29. Tittle,R.K., Sze,R., Ng,A., Nuckels,R.J., Swartz,M.E., Anderson,R.M., Bosch,J., Stainier,D.Y., Eberhart,J.K. and Gross,J.M. (2011) Uhrf1 and Dnmt1 are required for development and maintenance of the zebrafish lens. *Dev. Biol.*, **350**, 50–63.
30. Qin,Y., Wang,J., Gong,W., Zhang,M., Tang,Z., Zhang,J. and Quan,Z. (2014) UHRF1 depletion suppresses growth of gallbladder cancer cells through induction of apoptosis and cell cycle arrest. *Oncol. Rep.*, **31**, 2635–2643.
31. Jenkins,Y., Markovtsov,V., Lang,W., Sharma,P., Pearsall,D., Warner,J., Franci,C., Huang,B., Huang,J., Yam,G.C., *et al.* (2005) Critical role of the ubiquitin ligase activity of UHRF1, a nuclear

RING finger protein, in tumor cell growth. *Mol. Biol. Cell*, **16**, 5621–5629.
32. Chen,T., Hevi,S., Gay,F., Tsujimoto,N., He,T., Zhang,B., Ueda,Y. and Li,E. (2007) Complete inactivation of DNMT1 leads to mitotic catastrophe in human cancer cells. *Nat. Genet.*, **39**, 391–396.
33. Blais,A. and Dynlacht,B.D. (2007) E2F-associated chromatin modifiers and cell cycle control. *Curr. Opin. Cell Biol.*, **19**, 658–662.
34. Zhao,R., Choi,B.Y., Lee,M.H., Bode,A.M. and Dong,Z. (2016) Implications of genetic and epigenetic alterations of CDKN2A (p16(INK4a)) in cancer. *EBioMedicine*, **8**, 30–39.
35. Du,Q., Smith,G.C., Luu,P.L., Ferguson,J.M., Armstrong,N.J., Caldon,C.E., Campbell,E.M., Nair,S.S., Zotenko,E., Gould,C.M., *et al.* (2021) DNA methylation is required to maintain both DNA replication timing precision and 3D genome organization integrity. *Cell Rep.*, **36**, 109722.
36. Wang,S., Miller,S.R., Ober,E.A. and Sadler,K.C. (2017) Making it new again: insight into liver development, regeneration, and disease from zebrafish eesearch. *Curr. Top. Dev. Biol.*, **124**, 161–195.
37. Goessling,W. and Stainier,D.Y. (2016) Endoderm specification and liver development. *Methods Cell Biol.*, **134**, 463–483.
38. Chu,J. and Sadler,K.C. (2009) New school in liver development: lessons from zebrafish. *Hepatology*, **50**, 1656–1663.
39. Sladky,V.C., Knapp,K., Soratroi,C., Heppke,J., Eichin,F., Rocamora-Reverte,L., Szabo,T.G., Bongiovanni,L., Westendorp,B., Moreno,E., *et al.* (2020) E2F-family members engage the PIDDosome to limit hepatocyte ploidy in liver development and regeneration. *Dev. Cell*, **52**, 335–349.
40. Delgado,I., Fresnedo,O., Iglesias,A., Rueda,Y., Syn,W.K., Zubiaga,A.M. and Ochoa,B. (2011) A role for transcription factor E2F2 in hepatocyte proliferation and timely liver regeneration. *Am. J. Physiol. Gastrointest. Liver Physiol.*, **301**, G20–G31.
41. Wu,S.C., Kim,A., Gu,Y.J., Martinez,D.I., Zocchi,L., Chen,C.C., Lopez,J., Salcido,K., Singh,S., Wu,J., *et al.* (2022) UHRF1 overexpression promotes osteosarcoma metastasis through altered exosome production and AMPK/SEMA3E suppression. *Oncogenesis*, **11**, 51.
42. Mayhew,C.N., Carter,S.L., Fox,S.R., Sexton,C.R., Reed,C.A., Srinivasan,S.V., Liu,X., Wikenheiser-Brokamp,K., Boivin,G.P., Lee,J.S., *et al.* (2007) RB loss abrogates cell cycle control and genome integrity to promote liver tumorigenesis. *Gastroenterology*, **133**, 976–984.
43. Marjoram,L., Alvers,A., Deerhake,M.E., Bagwell,J., Mankiewicz,J., Cocchiaro,J.L., Beerman,R.W., Willer,J., Sumigray,K.D., Katsanis,N., *et al.* (2015) Epigenetic control of intestinal barrier function and inflammation in zebrafish. *Proc. Natl. Acad. Sci. U.S.A.*, **112**, 2770–2775.
44. Madakashira,B.P., Zhang,C., Macchi,F., Magnani,E. and Sadler,K.C. (2021) Nuclear organization during hepatogenesis in zebrafish requires Uhrf1. *Genes (Basel)*, **12**, 7.
45. Magnani,E., Macchi,F., Madakashira,B.P., Zhang,C., Alaydaroos,F. and Sadler,K.C. (2021) uhrf1 and dnmt1 loss induces an immune response in zebrafish livers due to viral mimicry by transposable elements. *Front. Immunol.*, **12**, 627926.
46. Knouse,K.A., Wu,J., Whittaker,C.A. and Amon,A. (2014) Single cell sequencing reveals low levels of aneuploidy across mammalian tissues. *Proc. Natl. Acad. Sci. U.S.A.*, **111**, 13409–13414.
47. Feng,S., Cokus,S.J., Zhang,X., Chen,P.Y., Bostick,M., Goll,M.G., Hetzel,J., Jain,J., Strauss,S.H., Halpern,M.E., *et al.* (2010) Conservation and divergence of methylation patterning in plants and animals. *Proc. Natl. Acad. Sci. U.S.A.*, **107**, 8689–8694.
48. Wang,S., Zhang,C., Hasson,D., Desai,A., SenBanerjee,S., Magnani,E., Ukomadu,C., Lujambio,A., Bernstein,E. and Sadler,K.C. (2019) Epigenetic compensation promotes liver regeneration. *Dev. Cell*, **50**, 43–56.
49. Chernyavskaya,Y., Mudbhary,R., Zhang,C., Tokarz,D., Jacob,V., Gopinath,S., Sun,X., Wang,S., Magnani,E., Madakashira,B.P., *et al.* (2017) Loss of DNA methylation in zebrafish embryos activates retrotransposons to trigger antiviral signaling. *Development*, **144**, 2925–2939.
50. Amsterdam,A., Nissen,R.M., Sun,Z., Swindell,E.C., Farrington,S. and Hopkins,N. (2004) Identification of 315 genes essential for early zebrafish development. *Proc. Natl. Acad. Sci. U.S.A.*, **101**, 12792–12797.
51. Mudbhary,R., Hoshida,Y., Chernyavskaya,Y., Jacob,V., Villanueva,A., Fiel,M.I., Chen,X., Kojima,K., Thung,S., Bronson,R.T., *et al.* (2014) UHRF1 overexpression drives DNA hypomethylation and hepatocellular carcinoma. *Cancer Cell*, **25**, 196–209.
52. Irion,U., Krauss,J. and Nusslein-Volhard,C. (2014) Precise and efficient genome editing in zebrafish using the CRISPR/Cas9 system. *Development*, **141**, 4827–4830.
53. Bollard,J., Miguela,V., Ruiz de Galarreta,M., Venkatesh,A., Bian,C.B., Roberto,M.P., Tovar,V., Sia,D., Molina-Sanchez,P., Nguyen,C.B., *et al.* (2017) Palbociclib (PD-0332991), a selective CDK4/6 inhibitor, restricts tumour growth in preclinical models of hepatocellular carcinoma. *Gut*, **66**, 1286–1296.
54. Prevo,R., Fokas,E., Reaper,P.M., Charlton,P.A., Pollard,J.R., McKenna,W.G., Muschel,R.J. and Brunner,T.B. (2012) The novel ATR inhibitor VE-821 increases sensitivity of pancreatic cancer cells to radiation and chemotherapy. *Cancer Biol. Ther.*, **13**, 1072–1081.
55. Evason,K.J., Francisco,M.T., Juric,V., Balakrishnan,S., Lopez Pazmino Mdel,P., Gordan,J.D., Kakar,S., Spitsbergen,J., Goga,A. and Stainier,D.Y. (2015) Identification of chemical inhibitors of beta-catenin-driven liver tumorigenesis in zebrafish. *PLoS Genet.*, **11**, e1005305.
56. Schmittgen,T.D. and Livak,K.J. (2008) Analyzing real-time PCR data by the comparative C(T) method. *Nat. Protoc.*, **3**, 1101–1108.
57. Inoue,D. and Wittbrodt,J. (2011) One for all–a highly efficient and versatile method for fluorescent immunostaining in fish embryos. *PLoS One*, **6**, e19713.
58. Stossi,F. and Singh,P.K. (2023) Basic image analysis and manipulation in ImageJ/Fiji. *Curr. Protoc*, **3**, e849.
59. Cordelieres,F.P. and Bolte,S. (2008), *ImageJ User & Developer Conference*, **174**, 181.
60. Zhao,X., Garcia,J., Royer,L.A. and Guo,S. (2022) Colocalization analysis for cryosectioned and immunostained tissue samples with or without label retention expansion microscopy (LR-ExM) by JACoP. *Biol. Protoc.*, **12**, e4336.
61. Bolger,A.M., Lohse,M. and Usadel,B. (2014) Trimmomatic: a flexible trimmer for Illumina sequence data. *Bioinformatics*, **30**, 2114–2120.
62. Supek,F., Bosnjak,M., Skunca,N. and Smuc,T. (2011) REVIGO summarizes and visualizes long lists of gene ontology terms. *PLoS One*, **6**, e21800.
63. Conway,J.R., Lex,A. and Gehlenborg,N. (2017) UpSetR: an R package for the visualization of intersecting sets and their properties. *Bioinformatics*, **33**, 2938–2940.
64. Zhang,J., Bellani,M.A., Huang,J., James,R.C., Pokharel,D., Gichimu,J., Gali,H., Stewart,G. and Seidman,M.M. (2021) Replication of the mammalian genome by replisomes specific for euchromatin and heterochromatin. *Front. Cell Dev. Biol.*, **9**, 729265.
65. Lee,S.H., Hao,E., Levine,F. and Itkin-Ansari,P. (2011) Id3 upregulates BrdU incorporation associated with a DNA damage response, not replication, in human pancreatic beta-cells. *Islets*, **3**, 358–366.
66. Rieck,S., Zhang,J., Li,Z., Liu,C., Naji,A., Takane,K.K., Fiaschi-Taesch,N.M., Stewart,A.F., Kushner,J.A. and Kaestner,K.H. (2012) Overexpression of hepatocyte nuclear factor-4alpha initiates cell cycle entry, but is not sufficient to

promote beta-cell expansion in human islets. *Mol. Endocrinol.*, **26**, 1590–1602.
67. Macaluso,M., Montanari,M., Noto,P.B., Gregorio,V., Bronner,C. and Giordano,A. (2007) Epigenetic modulation of estrogen receptor-alpha by pRb family proteins: a novel mechanism in breast cancer. *Cancer Res.*, **67**, 7731–7737.
68. Laderian,B. and Fojo,T. (2017) CDK4/6 inhibition as a therapeutic strategy in breast cancer: palbociclib, ribociclib, and abemaciclib. *Semin. Oncol.*, **44**, 395–403.
69. Pacek,M., Tutter,A.V., Kubota,Y., Takisawa,H. and Walter,J.C. (2006) Localization of MCM2-7, Cdc45, and GINS to the site of DNA unwinding during eukaryotic DNA replication. *Mol. Cell*, **21**, 581–587.
70. Tanaka,S., Tak,Y.S. and Araki,H. (2007) The role of CDK in the initiation step of DNA replication in eukaryotes. *Cell Div.*, **2**, 16.
71. Schmitz,M.L. and Kracht,M. (2016) Cyclin-dependent kinases as coregulators of inflammatory gene expression. *Trends Pharmacol. Sci.*, **37**, 101–113.
72. Ganz,J., Melancon,E., Wilson,C., Amores,A., Batzel,P., Strader,M., Braasch,I., Diba,P., Kuhlman,J.A., Postlethwait,J.H., *et al.* (2019) Epigenetic factors Dnmt1 and Uhrf1 coordinate intestinal development. *Dev. Biol.*, **455**, 473–484.
73. Milutinovic,S., Zhuang,Q.L., Niveleau,A. and Szyf,M. (2003) Epigenomic stress response - Knockdown of DNA methyltransferase 1 triggers an intra-S-phase arrest of DNA replication and induction of stress response genes. *J. Biol. Chem.*, **278**, 14985–14995.
74. Unterberger,A., Andrews,S.D., Weaver,I.C.G. and Szyf,M. (2006) DNA methyltransferase 1 knockdown activates a replication stress checkpoint. *Mol. Cell. Biol.*, **26**, 7575–7586.
75. Goll,M.G., Anderson,R., Stainier,D.Y., Spradling,A.C. and Halpern,M.E. (2009) Transcriptional silencing and reactivation in transgenic zebrafish. *Genetics*, **182**, 747–755.
76. Branzei,D. and Foiani,M. (2005) The DNA damage response during DNA replication. *Curr. Opin. Cell Biol.*, **17**, 568–575.
77. Lambert,S. and Carr,A.M. (2005) Checkpoint responses to replication fork barriers. *Biochimie*, **87**, 591–602.
78. Courtot,L., Hoffmann,J.S. and Bergoglio,V. (2018) The protective role of dormant origins in response to replicative stress. *Int. J. Mol. Sci.*, **19**, 11.
79. Reaper,P.M., Griffiths,M.R., Long,J.M., Charrier,J.D., MacCormick,S., Charlton,P.A., Golec,J.M.C. and Pollard,J.R. (2011) Selective killing of ATM- or p53-deficient cancer cells through inhibition of ATR. *Nat. Chem. Biol.*, **7**, 428–430.
80. Jung,J.K., Arora,P., Pagano,J.S. and Jang,K.L. (2007) Expression of DNA methyltransferase 1 is activated by hepatitis B virus X protein via a regulatory circuit involving the p16INK4a-cyclin D1-CDK 4/6-pRb-E2F1 pathway. *Cancer Res.*, **67**, 5771–5778.
81. D'Arcangelo,D., Tinaburri,L. and Dellambra,E. (2017) The role of p16(INK4a) pathway in human epidermal stem cell self-renewal, aging and cancer. *Int. J. Mol. Sci.*, **18**, 7.
82. Qin,W., Leonhardt,H. and Spada,F. (2011) Usp7 and Uhrf1 control ubiquitination and stability of the maintenance DNA methyltransferase Dnmt1. *J. Cell. Biochem.*, **112**, 439–444.
83. Felle,M., Joppien,S., Nemeth,A., Diermeier,S., Thalhammer,V., Dobner,T., Kremmer,E., Kappler,R. and Langst,G. (2011) The USP7/Dnmt1 complex stimulates the DNA methylation activity of Dnmt1 and regulates the stability of UHRF1. *Nucleic Acids Res.*, **39**, 8355–8365.
84. Arima,Y., Hirota,T., Bronner,C., Mousli,M., Fujiwara,T., Niwa,S., Ishikawa,H. and Saya,H. (2004) Down-regulation of nuclear protein ICBP90 by p53/p21Cip1/WAF1-dependent DNA-damage checkpoint signals contributes to cell cycle arrest at G1/S transition. *Genes Cells*, **9**, 131–142.
85. Merchut-Maya,J.M., Bartek,J. and Maya-Mendoza,A. (2019) Regulation of replication fork speed: mechanisms and impact on genomic stability. *DNA Repair (Amst.)*, **81**, 102654.
86. Maya-Mendoza,A., Moudry,P., Merchut-Maya,J.M., Lee,M., Strauss,R. and Bartek,J. (2018) High speed of fork progression induces DNA replication stress and genomic instability. *Nature*, **559**, 279–284.
87. Fu,H., Redon,C.E., Thakur,B.L., Utani,K., Sebastian,R., Jang,S.-M., Gross,J.M., Mosavarpour,S., Marks,A.B., Zhuang,S.Z., *et al.* (2021) Dynamics of replication origin over-activation. *Nat. Commun.*, **12**, 3448.
88. Bohly,N., Schmidt,A.K., Zhang,X., Slusarenko,B.O., Hennecke,M., Kschischo,M. and Bastians,H. (2022) Increased replication origin firing links replication stress to whole chromosomal instability in human cancer. *Cell Rep.*, **41**, 111836.
89. Koundrioukoff,S., Carignon,S., Techer,H., Letessier,A., Brison,O. and Debatisse,M. (2013) Stepwise activation of the ATR signaling pathway upon increasing replication stress impacts fragile site integrity. *PLoS Genet.*, **9**, e1003643.
90. Shechter,D. and Gautier,J. (2004) MCM proteins and checkpoint kinases get together at the fork. *Proc. Natl. Acad. Sci. U.S.A.*, **101**, 10845–10846.
91. Ge,X.Q. and Blow,J.J. (2010) Chk1 inhibits replication factory activation but allows dormant origin firing in existing factories. *J. Cell Biol.*, **191**, 1285–1297.
92. Park,S., Sater,A.H.A., Fahrmann,J.F., Irajizad,E., Cai,Y., Katayama,H., Vykoukal,J., Kobayashi,M., Dennison,J.B., Garcia-Manero,G., *et al.* (2022) Novel UHRF1-MYC axis in acute lymphoblastic leukemia. *Cancers (Basel)*, **14**, 17.
93. Jia,Y., Li,P., Fang,L., Zhu,H., Xu,L., Cheng,H., Zhang,J., Li,F., Feng,Y., Li,Y., *et al.* (2016) Negative regulation of DNMT3A de novo DNA methylation by frequently overexpressed UHRF family proteins as a mechanism for widespread DNA hypomethylation in cancer. *Cell Discov.*, **2**, 16007.
94. Kim,K.Y., Tanaka,Y., Su,J., Cakir,B., Xiang,Y., Patterson,B., Ding,J., Jung,Y.W., Kim,J.H., Hysolli,E., *et al.* (2018) Uhrf1 regulates active transcriptional marks at bivalent domains in pluripotent stem cells through Setd1a. *Nat. Commun.*, **9**, 2583.
95. Truong,L.N. and Wu,X. (2011) Prevention of DNA re-replication in eukaryotic cells. *J. Mol. Cell Biol.*, **3**, 13–22.
96. Aggarwal,P., Vaites,L.P., Kim,J.K., Mellert,H., Gurung,B., Nakagawa,H., Herlyn,M., Hua,X., Rustgi,A.K., McMahon,S.B., *et al.* (2010) Nuclear cyclin D1/CDK4 kinase regulates CUL4 expression and triggers neoplastic growth via activation of the PRMT5 methyltransferase. *Cancer Cell*, **18**, 329–340.
97. Aggarwal,P., Lessie,M.D., Lin,D.I., Pontano,L., Gladden,A.B., Nuskey,B., Goradia,A., Wasik,M.A., Klein-Szanto,A.J., Rustgi,A.K., *et al.* (2007) Nuclear accumulation of cyclin D1 during S phase inhibits Cul4-dependent Cdt1 proteolysis and triggers p53-dependent DNA rereplication. *Genes Dev.*, **21**, 2908–2922.
98. Kim,Y. and Kipreos,E.T. (2007) Cdt1 degradation to prevent DNA re-replication: conserved and non-conserved pathways. *Cell Div.*, **2**, 18.
99. Buss,H., Handschick,K., Jurrmann,N., Pekkonen,P., Beuerlein,K., Muller,H., Wait,R., Saklatvala,J., Ojala,P.M., Schmitz,M.L., *et al.* (2012) Cyclin-dependent kinase 6 phosphorylates NF-kappaB P65 at serine 536 and contributes to the regulation of inflammatory gene expression. *PLoS One*, **7**, e51847.
100. Ashraf,W., Ibrahim,A., Alhosin,M., Zaayter,L., Ouararhni,K., Papin,C., Ahmad,T., Hamiche,A., Mely,Y., Bronner,C., *et al.* (2017) The epigenetic integrator UHRF1: on the road to become a universal biomarker for cancer. *Oncotarget*, **8**, 51946–51962.
101. Liang,D., Xue,H., Yu,Y., Lv,F., You,W. and Zhang,B. (2015) Elevated expression of UHRF1 predicts unfavorable prognosis for patients with hepatocellular carcinoma. *Int. J Clin. Exp. Pathol.*, **8**, 9416–9421.

Received: August 7, 2023. **Revised:** December 12, 2023. **Editorial Decision:** December 31, 2023. **Accepted:** January 16, 2024
© The Author(s) 2024. Published by Oxford University Press on behalf of Nucleic Acids Research.
This is an Open Access article distributed under the terms of the Creative Commons Attribution-NonCommercial License (http://creativecommons.org/licenses/by-nc/4.0/), which permits non-commercial re-use, distribution, and reproduction in any medium, provided the original work is properly cited. For commercial re-use, please contact journals.permissions@oup.com